REMARKS

Rejection under 35 U.S.C. § 112

Claims 1-4, 6-15, 17-33 and 36-42 were rejected under 35 U.S.C. § 112, 1st paragraph, as containing subject matter not described so as to enable one skilled in the art to make or use the invention. The Office Action asserts that it would require undue experimentation to determine which materials other than CdS, CdSe and ZnO could be doped so as to be covered by the claims (paragraph 9, p. 5 of Office Action mailed 3-17-04). The Office Action further asserts that the working examples in the specification disclosing doped nanocrystals of CdS, CdSe and ZnO are insufficient to enable one skilled in the art to produce doped nanocrystals of other semiconductor materials consistent with the scope of the claims (paragraph 10, p. 6). In response to the Declaration of inventor Philippe Guyot-Sionnest, filed with the Amendment and Request for Reconsideration of January 22, 2004, the Office Action asserts that evidence of doped nanocrystals of a III-V semiconductor (InP) and of a IV-VI semiconductor (PbSe) is insufficient to show that Applicants' method will work for every semiconductor (paragraph 14, pp. 7-8).

The rejection of the claims under 35 U.S.C. § 112, 1st paragraph as not enabled is respectfully traversed. The specification provides adequate disclosure, both by specific example and broad terminology, to enable one skilled in the art to produce a doped semiconductor nanocrystal. This has been supported by a Declaration from the inventor, pursuant to 37 CFR 1.132, previously filed. Moreover, Applicants are submitting herewith yet another Declaration, pursuant to 37 CFR 1.132, from a separate researcher skilled in the art.

Level of Experimentation

With respect to the level of experimentation required to provide a doped nanocrystal from semiconductor materials other than CdS, CdSe and ZnO, Applicants refer to the attached Declaration of Arthur J. Nozik. In this Declaration, Prof. Nozik points out that he and other researchers have successfully applied the methods disclosed in the specification to other semiconductor materials. As noted in the Declaration, Prof. Nozik is a co-author of one of the articles cited in the Declaration, specifically Blackburn, Jeff L. et al. *J. Phys. Chem. B* **2003**, *107*, 102-109. In this article, *n*-type doped nanocrystals of InP, a III-V semiconductor, were prepared by treatment of InP nanocrystals with a solution of sodium biphenyl (page 103, left-hand column, in the paragraph having the heading "Preparation of *n*-Type Nanocrystals"). In discussing this article in the attached Declaration, Prof. Nozik also states that

> ... the synthesis of doped nanocrystals of InP did not require experimentation beyond a level that is customarily employed in the field of semiconductor nanocrystals.
> [Declaration of Arthur J. Nozik, paragraph 9, pp. 2-3]

Rather, the process reported in the article is substantially identical to specific methods described in the application, for example at page 6, lines 17-29 and at page 13, lines 5-12.

Clearly, the expansion of these methods to other materials has not required undue experimentation. Rather, the doping of other materials has been carried out using methods substantially identical to the methods disclosed in the specification. Moreover, the materials reported as doped using Applicants' methods include III-V semiconductors and IV-VI semiconductors, which are completely different classes from the II-VI semiconductors disclosed in Applicants' working examples.

Sufficiency of Disclosed Methods

With respect to the value of the working examples, Applicants respectfully point out that the disclosure in the specification regarding how to make and use the claimed invention is not limited to the working examples of CdS, CdSe and ZnO. As noted in MPEP 2164.08, with reference to *In re Marzocchi*,

> How a teaching is set forth, by specific example or by broad terminology, is not important.

It is this section of the MPEP, not MPEP 2164.01(b) as cited in the Office Action, that specifically addresses whether the disclosure bears a reasonable correlation to the entire scope of the claims. Taken as a whole, the disclosure of Applicants' specification, including the working examples, provides methods for making and using the claimed invention. Applicants respectfully note that the "EXAMPLES" section of the specification (pp. 11-15) is preceded by seven pages of general disclosure of the methods that may be followed to make and use the claimed invention (pp. 4-10).

Sufficiency of Evidence Presented in Declarations

With respect to the evidence now on the record that other semiconductors can be doped using the disclosed methods, Applicants submit that this evidence is directly applicable to the present question of enablement. The Office Actions have raised doubts as to whether semiconductors other than CdSe, CdS or ZnO, and/or semiconductors other than II-VI semiconductors, can be formed into doped semiconductor nanocrystals as claimed. The evidence on the record addresses these doubts by showing not only that other semiconductor materials can be doped in accordance with the disclosed methods (specifically InP and PbSe), but also that other classes of semiconductors can be doped in accordance with the disclosed methods (III-V and IV-VI, respectively). This evidence has been presented in the Declaration of inventor Philippe Guyot-Sionnest, filed with the Amendment and Request for Reconsideration of January 22, 2004, and in the Declaration of Arthur J. Nozik, filed herewith.

If the evidence on the record, both from Applicants' specification and from the Declarations, is insufficient to support a generic claim, then Applicants respectfully request the Office to indicate the amount and type of evidence that would be acceptable. Currently, the Office Action appears to be requesting a "basis by which the examiner can conclusively say that the applicant's method will work for *every* semiconductor compound" (p. 8, lines 1-2). The consequence of this evidentiary standard is that the Office is limiting the allowed subject matter to the working examples of the specification. Applicants respectfully point out that this conclusion is in conflict with the guidelines of the MPEP. Specifically, MPEP 2164.08 addresses this by quoting *In re Goffe*, 191 USPQ 429, 431 (CCPA 1976):

> To demand that the first to disclose shall limit his claims to what he has found will work or to materials which meet the guidelines specified for "preferred" materials in a process such as the one herein involved would not serve the constitutional purpose of promoting progress in the useful arts.

Thus, it is clearly improper to limit the present claims to the working examples of CdS, CdSe and ZnO. Applicants request that the specification, working examples and supplemental evidence on the record be fully considered, in view of these guidelines.

The subject matter of claims 1-4, 6-15, 17-33 and 36-42 is adequately described in the specification in such a way as to enable one skilled in the art to make and use the claimed invention. One skilled in the art would not be required to engage in undue experimentation to make and use the claimed invention. The specification provides both general and specific disclosure of methods to make and use the claimed invention in accordance with the scope of the claims. The record has been supplemented with evidence that the disclosed methods enable one skilled in the art to make and use the claimed invention without undue experimentation. Accordingly, the present claims fully meet the requirements of 35 U.S.C. § 112, 1st paragraph, and Applicants request that this rejection be withdrawn.

Conclusion

In conclusion, all of the grounds raised in the outstanding Office Action for rejecting the application are believed to be overcome or rendered moot based on the remarks above. Thus, it is respectfully submitted that all of the presently presented claims are in form for allowance. Should the Examiner feel a discussion would expedite the prosecution of this application, the Examiner is kindly invited to contact the undersigned.

Respectfully submitted,

9-17-04

Jonathan P. Taylor, Ph.D.
Registration No. 48,338
Agent for Applicant

BRINKS HOFER GILSON & LIONE
P.O. BOX 10395
CHICAGO, ILLINOIS 60610
(312) 321-4200

IN THE UNITED STATES PATENT AND TRADEMARK OFFICE

In re Application of: Philippe Guyot-Sionnest	
Serial No. 09/694,090	Examiner Nikolas J. Uhlir
Filing Date: October 19, 2000	Group Art Unit No. 1773
For DOPED SEMICONDUCTOR NANOCRYSTALS	

The Commissioner for Patents
P.O. Box 1450
Alexandria, VA 22313

DECLARATION PURSUANT TO 37 CFR 1.132

I, Arthur J. Nozik, declare as follows:

1. I am a Senior Research Fellow at the U.S. Department of Energy National Renewable Energy Laboratory (NREL) and a professor adjoint in the chemistry department at The University of Colorado, Boulder, CO. I received a Ph.D. from Yale University. Since 1993, I have been a Senior Editor of The Journal of Physical Chemistry.

2. As a professor and principal investigator for a research laboratory, I have worked in a variety of areas, including semiconductor quantum dots. I am a person of skill in the art in the field of semiconductor quantum dots and nanocrystals.

3. I am not being paid for this opinion.

4. I have reviewed and understand the contents of U.S. Patent Application Serial No. 09/694,090, entitled "Doped Semiconductor Nanocrystals" ("the application"), including the disclosure and the pending claims.

5. Having reviewed and understood the application, I believe that the application discloses methods for making and using a wide variety of doped semiconductor nanocrystals. I further believe that these methods are broadly applicable to semiconductor nanocrystals and are not limited to the specific CdS, CdSe and ZnO materials disclosed in the "EXAMPLES" section on pages 11-15 of the application, nor are the methods limited to the general class of II-VI semiconductors (also referred to as 2-6 semiconductors) encompassing these specific materials.

6. These methods are substantially similar to the methods described in Shim, W. et al. *J. Phys. Chem. B* **2001**, *105*, 2369 (attached as Appendix A) and in Shim, W. et al. *Nature* **2000**, *407*, 981 (attached as Appendix B).

7. I, as well as other researchers skilled in the art, now recognize the broad utility of the methods disclosed in the application for making doped semiconductor nanocrystals.

8. This recognition is evidenced by the citation of the above-referenced "Shim, W. et al." articles in more recent publications. For example:

(a) The publication Blackburn, Jeff L. et al. *J. Phys. Chem. B* **2003**, *107*, 102-109 (attached as Appendix C), reports the successful use of the methods disclosed in the application for preparing doped semiconductor nanocrystals from indium phosphide (InP), a III-V semiconductor material.

(b) The publication Wehrenberg, Brian L. et al. *J. Am. Chem. Soc.* **2003**, *125*, 7806-7807 (attached as Appendix D), the successful use of the methods disclosed in the application for preparing doped semiconductor nanocrystals from lead selenide (PbSe), a IV-VI semiconductor material.

9. The extension of the methods disclosed in the application to semiconductor materials other than II-VI semiconductors has not required undue experimentation. As a co-author of the Blackburn, Jeff L. et al. article referenced

above, I attest that the synthesis of doped nanocrystals of InP did not require experimentation beyond a level that is customarily employed in the field of semiconductor nanocrystals.

10. The disclosure of the application provides sufficient breadth and specificity to enable a researcher in this field to dope a semiconductor nanocrystal successfully, and without undue experimentation. The methods disclosed in the application can be used to dope a broad range of semiconductor types, including II-VI, III-V, and IV-IV, and this doping can be in the form of a hole or an electron. Doped semiconductor nanocrystals prepared by these methods can maintain the hole or electron in a quantum confined state at room temperature and in the absence of an applied electric field.

11. I declare that all statements made of my own knowledge are true and that all statements made on information and belief are believed to be true, and further that these statements were made with the knowledge that willful false statements and the like so made are punishable by fine or imprisonment, or both, under Section 1001 of Title 18 of the United States Code and that such willful false statements may jeopardize the validity of the above applications or any patent granted therein.

Arthur J. Nozik

Arthur J. Nozik

Sept 15, 2004

Date

Charge-Tunable Optical Properties in Colloidal Semiconductor Nanocrystals

Moonsub Shim,* Congjun Wang, and Philippe Guyot-Sionnest*

James Franck Institute, University of Chicago, Chicago, Illinois 60637

Received: September 29, 2000; In Final Form: November 21, 2000

The optical properties of colloidal semiconductor nanocrystals are found to be extremely sensitive to excess electrons. Electrons in the lowest quantum-confined state of the conduction band of CdSe and (CdSe)ZnS nanocrystals quench photoluminescence by several orders of magnitude, at the same time, leading to a strong, mid-infrared intraband absorption and bleaching of the interband exciton transitions. Surface electrons are also efficient in quenching photoluminescence, but a passivating layer of wider band gap ZnS can reduce their influence. The results suggest that single-electron switching of photoluminescence may be feasible with improved core/shell structures of semiconductor nanocrystals.

Introduction

Recent advances in nanometer-scale semiconductors have provided materials with many novel properties.[1,2] Device applications such as light-emitting diodes[3] and photovoltaic cells[4] have already been realized. Semiconductor nanocrystals prepared as colloids are a particularly interesting and important class of nanometer-scale materials especially due to the versatility with which they can be manipulated.[5] Depending on the capping molecules, these nanocrystals can be dispersed in a variety of solvents including those that are suitable for biological environment.[6,7] They can be manipulated into two- or three-dimensional superlattices.[8,9] Colloidal semiconductor nanocrystals are exceptionally well suited for studying photophysics and interactions in zero-dimensional materials, and there has been much progress in the control of size distribution,[5,10] shape,[11] and fluorescence efficiency[12−15] of nanocrystals of various semiconductors.

Recently, the effect of charges has received increased attention:

(i) Photoluminescence (PL) wandering of single nanocrystals[16,17] has been interpreted as resulting from the motion of surface charges and the associated Stark effect.[17]

(ii) Fluorescence intermittency (or blinking), again in single nanocrystals, has been proposed to arise from an Auger recombination process involving the remaining carrier, either an electron or a hole, after a single charge photoionization event.[18−20] Intraband spectroscopy[21] has indeed shown that electron-mediated Auger recombination occurs at a much faster rate than radiative recombination.[22,23]

(iii) An asymmetric surface charge distribution may also explain the large permanent dipole moments observed in wurtzite as well as zinc-blend neutral nanocrystals.[24]

(iv) Positively charged nanocrystals have been observed when adsorbed on gold substrates.[25]

(v) Charging energies between 0.1 and 0.2 eV have been measured from solution conductivity[24] as well as by scanning tunneling spectroscopy on single nanocrystals[26] in agreement with theoretical expectations.[27]

Therefore, charges are expected to be present and to have strong influence in the optical properties. However, there have been no studies of the optical properties upon charging. In particular, understanding the effects of charges on the photoluminescence may be relevant when semiconductor nanocrystals are utilized as luminescent labels in polar media. It may also help in elucidating the mechanism for blinking observed in single-nanocrystal fluorescence. Controlling the number of charges may lead to a possibility of fine-tuning and improving the optical properties of semiconductor nanocrystals. We present PL, UV/vis, and infrared studies of *n*-type and negatively charged colloidal semiconductor nanocrystals prepared by electron injection from a reducing species.[28]

Experimental Section

Synthesis of CdSe and (CdSe)ZnS Nanocrystals. Colloidal nanocrystals of CdSe are made in a similar manner as described in ref 5. (CdSe)ZnS (core)shell nanocrystals are prepared by the methods described in refs 12 and 13.

Preparation of *n*-Type Nanocrystals. The *n*-type nanocrystals are made as described in ref 28. Briefly, to 0.3 mL of dried and deaerated solution of nanocrystals with a small amount of TOPO (<5 mg/mL) in 2,2,4,4,6,8,8-heptamethylnonane is added ~10−50 μL of 1.2 M sodium biphenyl. The concentrations of nanocrystals are such that the optical density of the sample at the first exciton maximum is between 0.5 and 1.5 for 200 μm path length. Samples are prepared and filled into a cell in the absence of oxygen and closed in a N_2-filled glovebox. The cell is made of one CaF_2 window and a sapphire window separated by a Teflon spacer and is capped with Teflon stopcocks. For all experiments discussed here, samples are brought out of the glovebox after capping and left standing in ambient conditions during and between measurements. While the cell is solvent-tight, long exposure to air causes oxidation of the samples.

Optical Measurements. PL spectra are measured with Perkin-Elmer LS 50 B luminescence spectrometer. IR spectra are obtained with Nicolet Magna 560 FTIR spectrometer. UV/vis spectra are obtained with HP 8453 photodiode array spectrometer. All measurements are carried out at room temperature. No photodegradation has been observed under ambient lighting or spectrometer light sources.

* To whom correspondence should be addressed. E-mail: M.S., mshim@uchicago.edu; P.G.-S., pgs@uchicago.edu.

10.1021/jp0035683 CCC: $20.00
Published on Web 02/24/2001

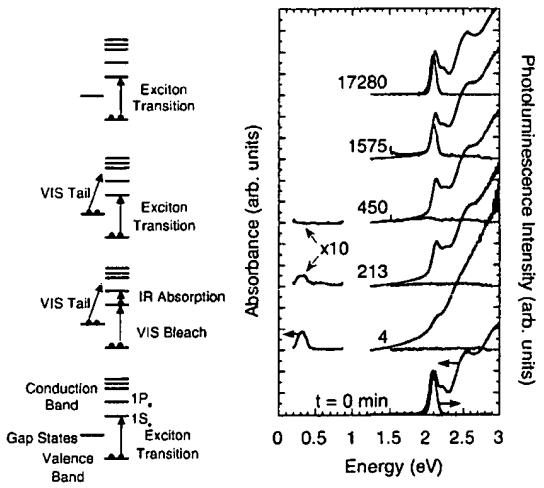

Figure 1. UV/vis and IR absorption and PL spectra of CdSe nanocrystals at different times after exposure to sodium biphenyl and schematic representations of the corresponding electron occupation. The spectrum corresponding to $t = 0$ min is before exposure to sodium biphenyl. Upon electron transfer from biphenyl radical anions, *n*-type nanocrystals exhibit strong mid-IR absorption along with a concurrent bleach of the exciton transitions in the visible. A complete quenching of PL is also observed. Note that middle 4 PL spectra are scaled 100 times for clarity.

Results and Discussion

After electrons are injected from the strongly reducing sodium biphenyl, a slow oxidation proceeds due to the ambient surrounding. What controls the oxidation rate and ultimately the long-term stability of the *n*-type material is a subject that we are currently investigating but do not fully understand yet. The oxidation rate is quenched at low temperatures and strongly increased in the presence of air or water. It also depends on the solvent, presumably due to its dryness and polarity. The kinetics of oxidation is sensitive to the material, faster for CdSe than ZnO, and generally faster for smaller sizes, in accord with their relative redox potentials.[28] Some decomposition can also occur as evidenced by a small blue-shift in the visible absorption peak observed in both CdSe and (CdSe)ZnS nanocrystals.

The evolution of the nanocrystal electron occupation after the electron injection is depicted on the left-hand side of Figure 1. A general evolution of the optical properties can be described as follows:

(1) In the highest observed charged state, electrons occupy the lowest conduction band state, $1S_e$, as evidenced by the strong, size-tunable IR absorption from $1S_e$ to $1P_e$. The corresponding population of the $1S_e$ state can be estimated from the observed bleach of the lowest exciton transition since a complete bleach of the first exciton arises for a two-electron occupation of $1S_e$. Similar bleach of the first exciton upon photoexcitation has previously been observed by microsecond to femtosecond transient absorption.[29-32] Here the bleach is observable over hours to days.

In addition to the quantum-confined states, there may be gap states. In these nanometer-size semiconductors, the most likely gap states are the surface states[33-35] rather than interior defects. The occupation of these surface states can lead to broadening and shifting of the optical spectrum via the Stark effect.[17] Furthermore, transitions from the surface states and the $1S_e$ state (to a lesser extent for the latter since most of their oscillator strength is in the $1S_e-1P_e$ transition) to higher quantum-confined excited states may lead to a broad optical absorption. Photoluminescence may be quenched by two distinct mechanisms: three-body Auger process involving electrons in the $1S_e$ state; hole trapping by the electron-rich surface followed by a nonradiative recombination.

(2) As oxidation proceeds, leaving electrons only in the surface states, the IR absorption and the bleach of the lowest exciton disappear. The shifts and broadening of the visible spectrum due to the Stark effect as well as the broad absorption from occupied surface states may remain. Again, PL may be quenched either by an Auger process or by hole trapping involving the occupied surface states.

Both CdSe and (CdSe)ZnS nanocrystals follow this two-step process. Differences arise from the better passivation of ZnS on CdSe resulting in smaller influence of surface trapped electrons.

CdSe Nanocrystals. The visible and IR absorption and the PL spectra of TOPO-capped CdSe nanocrystals before addition of sodium biphenyl are shown at the bottom of Figure 1. After addition of sodium biphenyl, a complete quenching of the band-edge luminescence is observed while there is a strong IR absorption ($t = 4$ min). The quenching remains after the IR absorption has completely disappeared ($t = 450$ min). The PL begins to recover well after ($t = 1575$ min) the complete decay of the IR absorption. Note that the middle four PL spectra are scaled 100 times that of the initial spectra for clarity.

To quantify the bleach of the exciton peaks and to separate out the contributions from broadening and Stark shifts as well as from the absorption tail, the spectra are fitted to a sum of Gaussians for the initial features and a rising power for the band-edge tail.[36] Figure 2B,C shows the results of this fitting procedure. Note that the biphenyl radical anions can be considered to be instantaneously oxidized in the time scale of the current measurements since the absorption feature of biphenyl radical anion at ~1.9 eV is not seen when they are exposed to the solution of nanocrystals. Therefore, no contribution of biphenyl radical anion to the visible spectra of nanocrystals is present.

Comparison of Figure 2A,B indicates that all three exciton peaks are bleached upon electron occupation of the $1S_e$ state of the conduction band. The first two exciton peaks have been assigned to transitions involving $1S_e$, and they are expected to have large and identical bleach.[37] The third peak overlaps with transitions involving both $1S_e$ and $1P_e$ states, and the bleach likely arises from the $1S_e$ contribution.

The average number of electrons occupying $1S_e$ state is estimated from the decrease in the area of the Gaussian fit corresponding to the first exciton transition normalized to account for a 2-electron maximum. For the sample in Figure 2B, the bleach in the first exciton transition gives an average of 1.4 ± 0.2 electrons in the $1S_e$ state immediately after exposure to sodium biphenyl. As shown in Figure 3, the visible bleach decay follows the IR absorption closely. This is expected since both the bleach and the IR absorption arise from electron occupation of $1S_e$ state. However, there is a residual 15% bleach which may be attributed to surface negative charges perturbing the electron and the hole states, possibly by mixing $1S_e$ and $1P_e$ states.

The broad band-edge tail is taken as a measure of the number of electrons in surface states because its intensity diminishes only after the $1S_e$ state is empty. When the PL recovers to half its initial value, about 5% of the band-edge tail remains. Assuming that one surface electron can completely quench the fluorescence, this point corresponds to about 0.5 electrons/

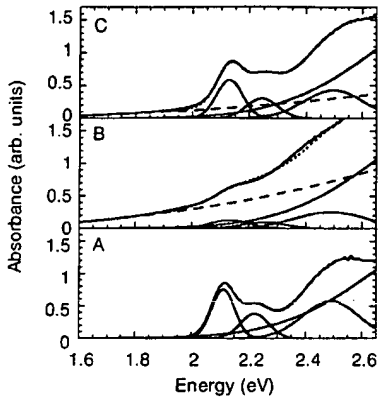

Figure 2. Demonstration of fitting procedure to quantify the changes in the visible absorption spectra of CdSe nanocrystals. The absorption spectrum before exposure to sodium biphenyl (A) is fitted to a sum of four Gaussians (shown below the spectrum). The absorption spectra after exposure to sodium biphenyl ((B) is 4 min and (C) is 450 min after) are also fitted to a sum of Gaussians and a rising power (dashed line) for the tail. The dotted lines are the fits and the Gaussians shown below each spectrum are reconstructed from the parameters of the fit. See ref 36 for details of the fitting procedure.

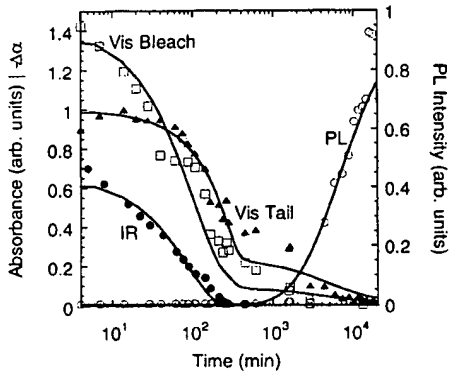

Figure 3. Time evolution of visible and IR properties of CdSe nanocrystals after electron transfer. IR absorption (filled circles) is the maximum absorption normalized for comparison. The visible bleach (open squares) is the difference in the area of the fitted Gaussian (see ref 36) for the first exciton transition then normalized for a 2-electron maximum. The visible absorption tail (filled triangles) is obtained from the coefficient of the rising power in the fit then normalized for comparison. Photoluminescence (open circles) is normalized with respect to initial PL intensity. The lines are from a simple model described in the text.

nanocrystal. Assuming further that the absorbance of the band-edge tail is linearly proportional to the number of electrons in surface states, we estimate that there are about 8−10 electrons in the surface states.

The logarithmic time dependence of the evolution of the optical properties suggests a titration process. A titration model[38] is then used to qualitatively fit the results in Figure 3 (solid lines). With an introduction of an oxidant (possibly water) at a constant rate, the chemical equilibrium between nanocrystals of different number of charges and the oxidant is solved. In this model, the nanocrystals can have at most 2 electrons in the $1S_e$ state and 8 surface electrons. The energies of the surface states are determined by a visual best fit to the data. The $1S_e$ state is at 0 eV, and there are a 4-electron state at −0.02 eV, a 2-electron state at −0.16 eV, and a 2-electron state at −0.3 eV. The oxidant is at −0.24 eV (if a charging energy identical for each electrons is introduced, the same equilibrium is obtained with an oxidant redox potential increased by the charging

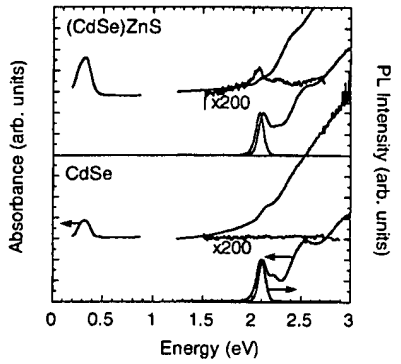

Figure 4. Comparison of the optical changes in ZnS-coated and uncoated CdSe nanocrystals upon electron transfer. Lower spectra in each half of the figure are before exposure to sodium biphenyl. Top spectra of each half are immediately (2−4 min) after.

energy). In this titration model, the PL is taken to be proportional to the concentration of nanocrystals with no charges. The bleach is proportional to the electron occupation of the $1S_e$ state plus a 2% contribution/surface charge. The IR absorption is proportional to the electron occupation of the $1S_e$ state divided by 2 so that it does not overlap with the bleach in the figure. The band-edge tail is proportional to the surface charges normalized to 1 at early times.

The small shift of the surface states with respect to $1S_e$ suggests that they have mostly Cd character. It is unclear at this stage whether the traps are intrinsic to the nanocrystals or are instead generated by the strongly reducing environments, removing some of the ligands for example. We also note that such shallow Cd surface states, even if present in the neutral nanocrystals, may not be optically observed. Indeed, hole states at the top of the valence band and Cd shallow surface states should have a very small overlap. Most of the transitions to the shallow surface states should involve hole states deeper in the valence band, thus being masked by the stronger exciton transitions. It should also be noted that the titration model is only meant to be a guideline in describing the changes in the optical properties of reduced nanocrystals and not to be taken as a definitively quantitative analysis of the observations.

(CdSe)ZnS (Core)shell Nanocrystals. Figure 4 compares the changes in the optical properties of ZnS coated and uncoated CdSe nanocrystals of similar core size as they are made *n*-type. Notice that while there is approximately the same amount of visible bleach of the first two exciton peaks, (CdSe)ZnS exhibits much less of the band-edge tail. Analysis of the first exciton bleach gives about 1.9 electrons initially in the $1S_e$ state. The recovery of the visible bleach follows the IR absorption decay closely (Figure 5). When PL recovers to 50%, there is about 30% of the band-edge tail remaining, which is indicative of 2−4 electrons in surface states, significantly less than that of uncoated CdSe. This observation that (CdSe)ZnS has, on average, less electron traps than CdSe is consistent with the improved luminescence afforded by the ZnS coating[12] and with the expectation that the Zn-derived surface states should be higher in energy than the core conduction band minimum.

For *n*-type (CdSe)ZnS, although the $1S_e$ state is nearly fully populated, the quantum yield is about 10^{-3} relative to the neutral state. This small but nonzero quantum yield is consistent with an Auger rate of ~100 ps (in the 2 electron−hole pair limit for ~5 nm diameter CdSe nanocrystals[22,23]) and a fluorescence lifetime of 100 ns. It is also significant that the PL recovery begins when there is about half of the initial IR absorption or ~1 electron in the $1S_e$ state. In fact, the PL from nanocrystals

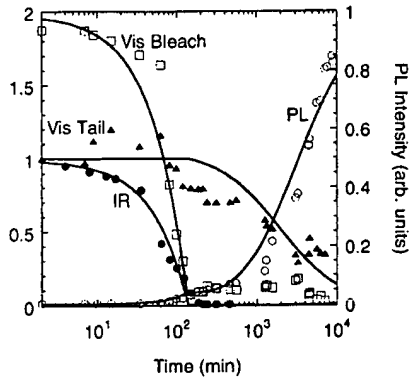

Figure 5. Time evolution of visible and IR properties of (CdSe)ZnS (core)shell nanocrystals after electron transfer from sodium biphenyl. The same description as Figure 3 caption applies.

with remaining surface charges is about 4% of the original PL and at least 2 orders of magnitude larger than in uncoated CdSe nanocrystals with surface charges. This behavior can be understood from the wider band gap ZnS reducing the coupling between surface states and core states leading to a weaker PL quenching. Alternatively, the 4% PL level can be due to 4% of the nanocrystals having no surface band gap states to accommodate excess electrons. In either case, the additional quenching of the PL upon occupation of the $1S_e$ state is a strong support for electron-mediated Auger recombination since it is unlikely to be due to the $1S_e$ electrons increasing the hole trapping rate.

The lines shown in Figure 5 are the results of identical equilibrium considerations as described in the previous subsection except that only a 2-electron deep trap is considered ($1S_e$ state at 0 eV, a 2-electron trap state at −0.3 eV, and the oxidant redox potential at −0.24 eV). We neglect the contribution of surface charges to the visible bleach, and a 4% PL relative efficiency for nanocrystals with only surface charges must be included to account for the PL recovery.

Photoluminescence Properties. A comparison of the results of CdSe and (CdSe)ZnS nanocrystals strongly suggests that the electron-mediated Auger recombination process is dominant when the electron is in $1S_e$. The mechanism by which the excess surface electrons quench the PL could, however, be a combination of both Auger and hole-trap mechanisms. The hole-trap mechanism requires a nonradiative transition from the valence band to the electron surface states. These are derived from the Cd surface atoms, and they should be about 2 eV above the valence band. The trapping rate may then be too slow. On the other hand, the strong absorption tail at the band edge, if arising truly from transitions between the surface electrons and the interior states, implies that an Auger process should be efficient.

It is interesting to note that water-soluble nanocrystals (e.g. silica-coated (CdSe)CdS[6] and mercaptoalkanoic acid capped (CdSe)ZnS[7]) exhibit reduced quantum yields relative to their TOPO-capped counterparts in nonpolar organic solvents. Due to the lower charging energy in a polar medium, these nanocrystals are more prone to surface charges which may explain the reduced fluorescence efficiencies.

Conclusions

We have shown that electron transfer causes dramatic changes in the optical properties of colloidal semiconductor nanocrystals. In both CdSe and (CdSe)ZnS nanocrystals, there is a strong IR absorption corresponding to the $1S_e-1P_e$ transition when they are made *n*-type. Concurrent bleach of the exciton transitions accompanies the IR absorption. The photoluminescence is strongly quenched in these negatively charged nanocrystals. We have found that both surface charges and delocalized electrons lead to strong quenching, the latter via an Auger process. These observations suggest that one simple way of controlling the optical properties is to control the number of electrons or the Fermi level in semiconductor nanocrystals. Improved surface passivation or electron injection conditions may lead to the possibility that the fluorescence of semiconductor nanocrystals can be fully quenched by injection of a single electron.

Acknowledgment. This work was funded by the National Science Foundation under Grant No. DMR-9731642. We made use of the MRSEC Shared Facilities supported by the National Science Foundation under Grant No. DMR-9400379.

References and Notes

(1) Nirmal, M.; Brus, L. E. *Acc. Chem. Res.* **1999**, *32*, 407.
(2) Alivisatos, A. P. *Science* **1996**, *271*, 933.
(3) Colvin, V. L.; Schlamp, M. C.; Alivisatos, A. P. *Nature* **1994**, *370*, 354. Dabbousi, B. O.; Bawendi, M. G.; Onitsuka, O.; Rubner, M. F. *Appl. Phys. Lett.* **1995**, *66*, 1316.
(4) O'Regan, B.; Grätzel, M. *Nature* **1991**, *353*, 737.
(5) Murray, C. B.; Norris, D. J.; Bawendi, M. G. *J. Am. Chem. Soc.* **1993**, *115*, 8706.
(6) Bruchez, M., Jr.; et al. *Science* **1998**, *281*, 2013.
(7) Chan, W. C.; Nie, S. *Science* **1998**, *281*, 2016.
(8) Murray, C. M.; Kagan, C. R.; Bawendi, M. G. *Science* **1995**, *270*, 1335.
(9) Collier, C. P.; Vossmeyer, T.; Heath, J. R. *Annu. Rev. Phys. Chem.* **1998**, *43*, 371.
(10) Micic, O. I.; et al. *J. Phys. Chem.* **1994**, *98*, 4966.
(11) Peng, X.; et al. *Nature* **2000**, *404*, 59.
(12) Hines, M. A.; Guyot-Sionnest, P. *J. Phys. Chem.* **1996**, *100*, 468.
(13) Dabbousi, B. O.; Rodriguez-Viejo, J.; Mikulec, F. V.; Heine, J. R.; Mattoussi, H.; Ober, R.; Jensen, K. F.; Bawendi, M. G. *J. Phys. Chem. B* **1997**, *101*, 9463.
(14) Peng, X.; et al. *J. Am. Chem. Soc.* **1997**, *119*, 7019.
(15) Cao, Y.; Banin, U. *Angew. Chem., Int. Ed. Engl.* **1999**, *38*, 3692.
(16) Blanton, S. A.; Hines, M. A.; Guyot-Sionnest, P. *Appl. Phys. Lett.* **1996**, *69*, 3905.
(17) Empedocles, S.; Bawendi, M. G. *J. Phys. Chem.* **1999**, *103*, 1826.
(18) Nirmal, M.; et al. *Nature* **1996**, *383*, 802.
(19) Banin, U.; Bruchwz, M.; Alivisatos, A. P.; Ha, T.; Chemla. D. S. *J. Chem. Phys.* **1999**, *110*, 1195.
(20) Kuno, M.; Fromm, D. P.; Hamann, H. F.; Gallagher, A.; Nesbitt, D. J. *J. Chem. Phys.* **2000**, *112*, 3117.
(21) Guyot-Sionnest, P.; Hines, M. A. *Appl. Phys. Lett.* **1998**, *72*, 686.
(22) Guyot-Sionnest, P.; Shim, M. S.; Matranga, C.; Hines, M. A. *Phys. Rev. B* **1999**, *60*, R2181.
(23) Klimov, V. I.; et al. *Science* **2000**, *287*, 1011.
(24) Shim, M.; Guyot-Sionnest, P. *J. Chem. Phys.* **1999**, *111*, 6955.
(25) Krauss, T. D.; Brus, L. E. *Phys. Rev. Lett.* **1999**, *83*, 4840.
(26) Banin, U.; Cao, Y.; Katz, D.; Millo, O. *Nature* **1999**, *400*, 542.
(27) Franceschetti, A.; Zunger, A. *Appl. Phys. Lett.* **2000**, *76*, 1731.
(28) Shim, M.; Guyot-Sionnest, P. *Nature* **2000**, *407*, 981.
(29) Dimitrijevic, N. M.; Kamat, P. V. *J. Phys. Chem.* **1987**, *91*, 2096.
(30) Woggon, U.; Giessen, H.; Fluegel, B.; Peyghambarian, N. *Phys. Rev. B* **1996**, *54*, 17681.
(31) Burda, C.; Link, S.; Green, T. C.; El-Sayed, M. A. *J. Phys. Chem. B* **1999**, *103*, 10775.
(32) Klimov, V. I. *J. Phys. Chem. B* **2000**, *104*, 6112.
(33) Sercel, P.; Efros, Al. L.; Rosen, M. *Phys. Rev. Lett.* **1999**, *83*, 2394.
(34) Fu, H.; Zunger, A. *Phys. Rev. B* **1997**, *56*, 1496.
(35) Pokrant, S.; Whaley, K. B. *Eur. Phys. J. D* **1999**, *6*, 255.
(36) The UV/vis absorption spectrum of nanocrystals before exposure to sodium biphenyl is fitted to a sum of four Gaussians as shown in Figure 3A. The fourth Gaussian at the highest energy (dashed line in Figure 3A) is to take the UV rise in the absorption features into account. Using the parameters of this fit, the amplitude, the position, and the width of this fourth Gaussian is held fixed and the first three are allowed to vary in magnitude, position, and width to account for the bleach, Stark shift, and broadening in the UV/vis spectra of *n*-type and negatively charged nanocrystals. The changes in widths of these three Gaussians are constrained to be the same, and the shifts in the positions of the first and second exciton peaks are proportional to the ratio of their original positions with respect to the bulk band gap. That is, if the shift in the first exciton peak is ΔE, the

shift in the next exciton peak is constrained to be $\Delta E \times (E_2 - E_g)/(E_1 - E_g)$. E_1 and E_2 are the positions of the first and the second exciton peaks, respectively, of the nanocrystals before exposure to sodium biphenyl. E_g is the bulk band gap. The third peak does not follow the same proportional shift due to the fact that it is composed of several different transitions. There is also an additional term of the form constant $\times (E - E_g/2)^{2.5}$ to account for the visible tail.

(37) Norris, D. J.; Bawendi, M. G. *Phys. Rev. B* **1996**, *53*, 16338.

(38) In this titration model, the partition function of CdSe nanocrystals with a 2-electron $1S_e$ state (0 eV), a 4-electron surface trap state (−0.02 eV), a 2-electron trap state (−0.16 eV), and a 2-electron trap state (−0.3 eV) is $Z = \Sigma_{j=0}{}^{10} \exp[-(E_j - j\mu)/kT]$, where E_j is the energy of the nanocrystals with j electrons. The oxidant, linearly introduced in time, has a partition function $Z_0 = 1 + \exp[-(E_0 - j\mu)/kT]$ between its reduced and oxidized form. Given an initial μ, the concentration of nanocrystals, the rate of introduction of the oxidant, the time evolution of μ, and the concentration of all the species are uniquely determined. The evolution of IR absorption, visible bleach and tail, and PL can then be reproduced as described in the text.

Acknowledgements

We thank the NASA Planetary Astronomy programme for financial support of this research and the NASA Keck Telescope Allocation Committee for consistent allocation of telescope time.

Correspondence and requests for materials should be addressed to S.C.T. (e-mail: tegler@proto.phy.nau.edu).

n-type colloidal semiconductor nanocrystals

Moonsub Shim & Philippe Guyot-Sionnest

James Franck Institute, University of Chicago, 5640 S. Ellis Avenue, Chicago, Illinois 60637, USA

Colloidal semiconductor nanocrystals[1,2] combine the physical and chemical properties of molecules with the optoelectronic properties of semiconductors. Their colour is highly controllable, a direct consequence of quantum confinement on the electronic states[3]. Such nanocrystals are a form of 'artificial atoms' (ref. 4) that may find applications in optoelectronic systems such as light-emitting diodes[5,6] and photovoltaic cells[7], or as components of future nanoelectronic devices. The ability to control the electron occupation (especially in n-type or p-type nanocrystals) is important for tailoring the electrical and optical properties, and should lead to a wider range of practical devices. But conventional doping by introducing impurity atoms has been unsuccessful so far: impurities tend to be expelled from the small crystalline cores (as observed for magnetic impurities[8]), and thermal ionization of the impurities (which provides free carriers) is hindered by strong confinement. Here we report the fabrication of n-type nanocrystals using an electron transfer approach commonly employed in the field of conducting organic polymers[9]. We find that semiconductor nanocrystals prepared as colloids can be made n-type, with electrons in quantum confined states.

Electron transfer in and out of nanocrystals has been a subject of study for many years, mostly in the context of photochemistry and photovoltaics[10]. However, there has never been any conclusive evidence that injected electrons could be placed in the Lowest Unoccupied Quantum-Confined Orbital (we will use the acronym LUQCO) which is the essence of making n-type nanocrystals. Instead, the electrons were most probably transferred to trap states. Reducing the nanocrystals such that they are n-type requires the absence or saturation of electron traps and a slow kinetics towards oxidation. This may seem hopeless given the large surface area of the nanocrystals and the possible presence of many dangling bonds. However, the conduction band minimum of many semiconductors lies near the reduction potential of hydrogen[11], well below the reduction potential of alkali metals (for example, the reduction potential of Na = −2.71 V versus SHE). While quantum confinement shifts the energy levels of the conduction band higher (relative to the bulk), that shift is typically less than 1 eV for most sizes of quantum dots studied. Therefore it should be feasible to inject electrons into semiconductor nanocyrstals with alkali metals in a manner similar to organic polymers[9], C_{60} (ref. 12) and carbon nanotubes[13]. Using surface-passivated nanocrystals in anhydrous and de-aerated solutions, we have observed successful electron transfer from sodium biphenyl to the LUQCO of colloidal semiconductor nanocrystals, making them the first n-type nanocrystals. The radical anion of biphenyl acts as the charge shuttle. The n-type nanocrystals can also be obtained by simply exposing a solution of nanocrystals to chunks of sodium. However, this process typically takes several days owing to the low mobility of the nanocrystals.

To ascertain that the electrons are successfully placed in the LUQCO of the nanocrystals, rather than merely charging them by occupation of surface states, infrared spectroscopy of the $1S_e$–$1P_e$ intraband transition has been used. As seen in the inset of Fig. 1, if an electron is successfully transferred into the LUQCO (labelled $1S_e$ for a spherical nanocrystal), a strong electronically allowed infrared transition to the next higher state (labelled $1P_e$) must appear. At the same time, a bleach of the exciton transition must occur as a result of the occupation of the $1S_e$ state. Therefore a combination of infrared and optical spectroscopy provides a rigorous diagnosis of the n-type character of the nanocrystals.

In Fig. 1, infrared and visible absorption spectra of 5.2-nm CdSe nanocrystals before (dotted line) and about 1 minute after (solid line) the addition of sodium biphenyl reagent are shown. Upon charge transfer, the first and the second exciton peaks at 2.07 and 2.18 eV, respectively, are strongly bleached and broadened. Broadening is expected if there are charges that can shift the exciton energy by the Stark effect and this can also lead to an apparent blue shift. As the charges may reside in surface states and/or in the delocalized $1S_e$ state, the changes in the visible absorption indicate that electron transfer may possibly have occurred but do not guarantee that the nanocrystals are n-type. The true n-type character of the nanocrystals is unambiguously confirmed by the appearance of the $1S_e$–$1P_e$ infrared absorption arising at 0.3 eV.

The size-dependence of this $1S_e$–$1P_e$ transition in the n-type nanocrystals is similar to photoexcited nanocrystals[14,15]. Figure 2 shows infrared absorption spectra corresponding to the $1S_e$–$1P_e$ transition in n-type CdSe nanocrystals of different sizes capped with trioctylphosphine oxide (TOPO). Figure 3 compares the size dependence of the $1S_e$–$1P_e$ transition observed in n-type CdSe nanocrystals (filled circles) to the effective mass calculation[16] (solid line) and shows a fair agreement. A previously reported $1S_e$–$1P_e$ transition observed in optically excited CdSe nanocrystals[14] (open triangles) as well as for n-type CdSe nanocrystals with various caps (filled diamonds) are also shown in Fig. 3. As we expected, whether

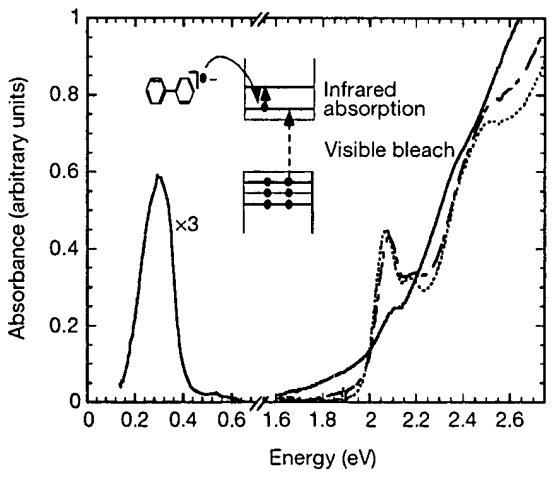

Figure 1 Absorption spectra of CdSe nanocrystals. Spectra are shown before (dotted line), immediately after (solid line), and 27 hours after (dashed line) the addition of sodium biphenyl reagent. The concurrent optical bleach of the first two exciton transitions and the appearance of the infrared absorption are clearly seen. The blue-shift of the optical spectra after the disappearance of the infrared absorption suggests that the n-type nanocrystals decompose by loss of the outermost layer of the semiconductor. Typically, n-type nanocrystals are made by addition of sodium biphenyl to a dried and degassed solution of nanocrystals in heptamethylnonane (~0.1 mM in nanocrystals and ~50 mM in sodium biphenyl). Small amounts of TOPO (<5 mg ml^{-1}) can be added to prevent precipitation.

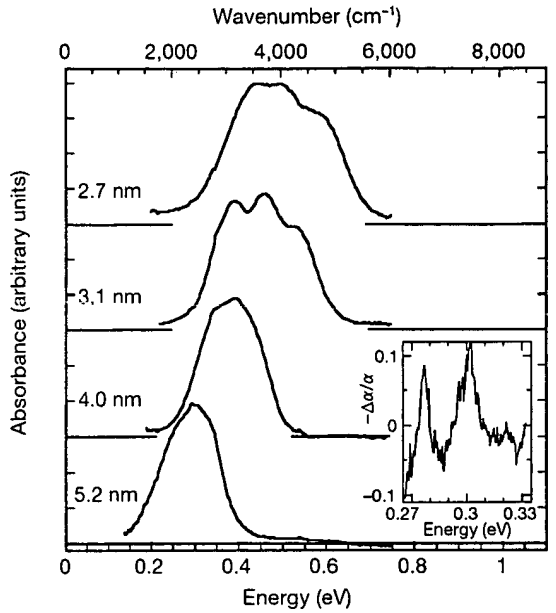

Figure 2 Infrared absorption spectra of n-type CdSe nanocrystals capped with TOPO. The sizes correspond to the diameter of the core semiconductor. Between 0.35 to 0.37 eV, the solvent C-H sketch blocks out the infrared source and the absorbance in this range is omitted for clarity. The $1S_e-1P_e$ transitions in the smallest two sizes of n-type CdSe nanocrystals show three distinct features, possibly arising from the lifting of threefold degeneracy of $1P_e$ states. The inset is the infrared hole-burning spectrum of 5.2-nm samples at 20 K. The main bleach is at the pump frequency, 0.3 eV, and the strong phonon replica appears at 0.275 eV. The longitudinal optical (LO) phonon for bulk CdSe is 26 meV. α, absorbance.

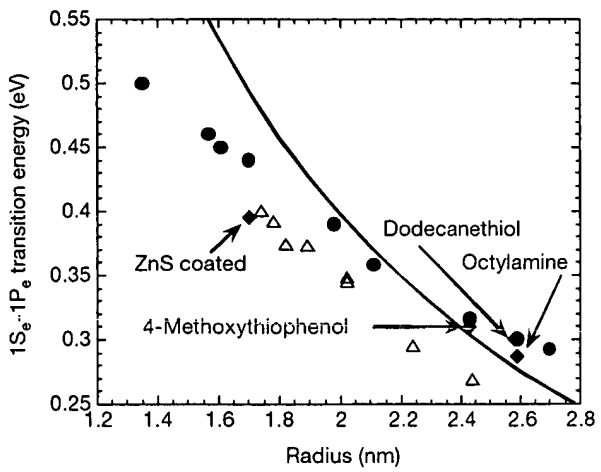

Figure 3 Experimental $1S_e-1P_e$ transition energy of n-type CdSe nanocrystals. The transition energies of the nanocrystals capped with TOPO (filled circles) and optically excited nanocrystals (open triangles) are compared to effective mass calculation (solid line). The filled diamonds are for n-type CdSe nanocrystals with various capping groups as indicated. The infrared absorption band is easily tuned with size and its position can be readily determined from bulk properties.

the surface capping group introduces hole traps (for example, 4-methoxythiophenol) or removes these traps (for example, ZnS coating), the electron injection process to produce n-type semiconductor nanocrystals is not affected.

The $1S_e-1P_e$ transitions are inhomogeneously broadened mostly from a distribution of sizes ($\sigma \approx 5$ to 8%). The linewidths are about 30% larger than that of the first exciton peak in the visible spectra of the neutral nanocrystals (for samples shown in Fig. 2, the infrared full-widths at half-maximum (FWHM) are 0.26, 0.22, 0.15 and 0.14 eV and the visible FWHM values are 0.19, 0.16, 0.14 and 0.11 eV from the smallest to the largest sizes, respectively). Low-temperature infrared hole-burning spectra of n-type CdSe nanocrystals confirm that the linewidths are dominated by the size distribution. At 20 K, an upper limit of 5 meV is obtained for the homogeneous linewidth (M.S. and P.G.-S., unpublished work) of 5.2-nm nanocrystals (see Fig. 2 inset).

The $1S_e-1P_e$ transition in n-type CdSe nanocrystals presents a very large absorbance, comparable to the first exciton transition. In Fig. 1, it is nearly one half that of the first exciton transition in the visible. Infrared absorbance almost as large as the first exciton transition has been observed in 5.4-nm CdSe nanocrystals (absorbance at 2.05 eV was 0.423 before sodium biphenyl addition compared to peak absorbance at 0.3 eV, which was 0.395). Using the molar extinction coefficients of the visible absorption spectra[17], the infrared molar absorptivity for this sample is about $0.8 \times 10^6\ M^{-1}\ cm^{-1}$.

The long-term stability of the n-type nanocrystals is strongly affected by the presence of impurities, exposure to air and the dryness of the solution. The decay is probably due to further oxidation and decomposition. In n-type CdSe nanocrystals, the $1S_e-1P_e$ transition decays within 30 minutes to 24 hours (from the smallest to the largest sizes, respectively) at room temperature. If the solution of nanocrystals and biphenyl anions is intentionally exposed to air, decay occurs within minutes. The stability of the n-type nanocrystals is also strongly temperature-dependent because at 20 K the samples appear to be stable indefinitely (in excess of five weeks). Several hours to days after the complete decay of the infrared absorption, there is a recovery of the optical bleach. After recovery, the nanocrystals are of smaller sizes as indicated by the blue-shift of the optical absorption features shown in Fig. 1 (dashed line). The blue-shift from 2.07 to 2.08 eV corresponds to a reduction in size of about 2 Å in diameter. We note that the infrared absorption and the optical bleach can be 'turned on' again by the addition of more sodium biphenyl reagent.

If no excess capping molecules (TOPO and trioctylphosphine (TOP) for samples in Figs 1 and 2) are present in the solution, a slow precipitation of the nanocrystals occurs. We note that excess TOPO (without excess TOP) present in solution prevents this slow precipitation. As the reduction potential of Cd/Cd^{2+} is −0.403 V versus the standard hydrogen electrode (SHE) near or below the LUQCO of CdSe nanocrystals, the most likely pathway for the decomposition of n-type CdSe nanocrystals is by oxidation with loss of electrons in Cd/TOPO complexes in solution. As expected, smaller n-type nanocrystals with a larger degree of confinement are less stable. Determining which systems can be made n-type by the electron transfer method and the thermodynamic stability of the n-type nanocrystals may simply be approached by looking at the reduction potential of the nanocrystals and of their constituent elements. For example, n-type ZnSe nanocrystals may be less stable because the reduction potential of Zn/Zn^{2+} is −0.762 V versus SHE whereas the conduction band minimum of bulk ZnSe is near −1.5 V versus SHE[11]. On the other hand, ZnO, with its valence band minimum near the reduction potential of hydrogen[11], should be an excellent candidate. In fact, charge transfer to ZnO nanocrystals has been previously investigated by electrochemistry but the ultraviolet–visible spectra could not distinguish between electron transfer to trap states or to the LUQCO[18,19].

Figure 4 shows the infrared absorption spectra of n-type ZnO, CdS and CdSe nanocrystals prepared by the electron transfer method. The visible bleach and tail are also observed in all three types of nanocrystals. The relatively broader infrared absorption band of ZnO may be attributed to a larger size distribution ($\sigma \approx 25\%$) as well as to a stronger electron–phonon interaction. The insets of Fig. 4 are the corresponding time evolution of the

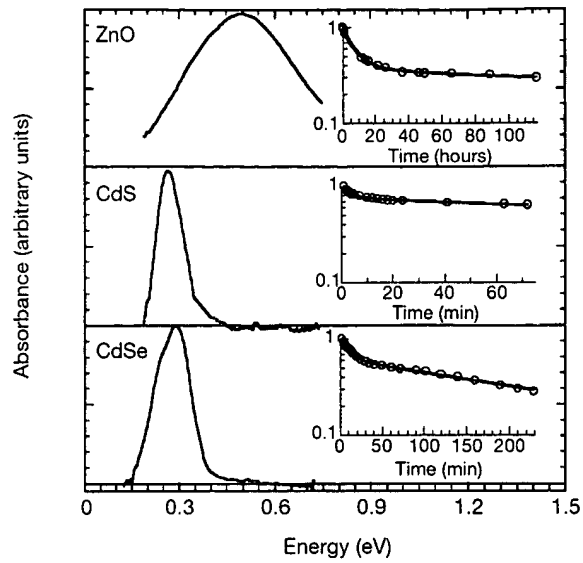

Figure 4 Infrared absorption spectra of n-type ZnO (4.4 nm), CdS (7 nm) and CdSe (5.4 nm) nanocrystals capped with TOPO. The insets are the corresponding time evolution of the infrared absorbance maximum normalized for comparison. We note that the *x*-axis of the inset for ZnO is in hours.

infrared absorption maximum. As expected from the relative reduction potentials of the semiconductor and of the constituent elements, n-type ZnO nanocrystals are more stable than CdS and CdSe. At room temperature, approximately 30% of the initial infrared absorption is observed 5 days after the initial preparation of n-type ZnO nanocrystals, whereas the infrared absorption completely decays in less than 2 days for both CdS and CdSe nanocrystals. The intrinsic limit of this electron injection method should be the point at which the sum of the confinement energy, the charging energy and the position of the conduction band minimum reaches the reduction potential of the reducing species.

One of the advantageous properties of quantum dots prepared as colloids is the organic capping layer. The readily exchangeable organic surfactants allow for a versatile manipulation of nanocrystals in many different environments. For example, recapping nanocrystals with organic functional groups that are compatible with physiological environments has shown that nanocrystals can be useful biological tags[20,21]. The electron injection into the LUQCO is also achieved in nanocrystals with different capping groups as indicated in Fig. 3. As long as the capping layer does not introduce electron traps within the band gap, this method should be applicable. The capping layer also provides an avenue to improve the long-term stability of n-type nanocrystal (for example, binding of the cation to the surface and core/shell structures).

Colloidal semiconductor nanocrystals of various materials (CdSe, CdS and ZnO) can be reduced to n-type by Na or biphenyl radical anions with electrons occupying the quantum confined states of the conduction band. A stability of hours to days at room temperature is observed and improvements are likely in the future. We have shown how electron occupation of the $1S_e$ state dramatically affects the optical properties, creating the possibility for strong electrochromic response in the visible and mid-infrared. The conductivity of films of n-type nanocrystals is one of the most interesting aspects to investigate, owing to the possibility of enhanced inter-nanocrystal electron transfer that may lead to photovoltaic or electronic applications. In general, the control of the Fermi level should be important in future applications of colloidal semiconductor nanocrystals and the electron transfer method may be the most viable approach in the nanometer length scale with strong confinement. □

Received 22 June; accepted 6 September 2000.

1. Nirmal, M. & Brus, L. E. Luminescence photophysics in semiconductor nanocrystals. *Acc. Chem. Res.* **32**, 407–414 (1999).
2. Alivisatos, A. P. Semiconductor clusters, nanocrystals, and quantum dots. *Science* **271**, 933–937 (1996).
3. Murray, C. B., Norris, D. J. & Bawendi, M. G. Synthesis and characterization of nearly monodisperse CdE (E = S, Se, Te) semiconductor nanocrystallites. *J. Am. Chem. Soc.* **115**, 8706–8715 (1993).
4. Ashoori, R. C. Electrons in artificial atoms. *Nature* **379**, 413–419 (1996).
5. Colvin, V. L., Schlamp, M. C. & Alivisatos, A. P. Light-emitting diodes made from cadmium selenide nanocrystals and a semiconducting polymer. *Nature* **370**, 354–357 (1994).
6. Dabbousi, B. O., Bawendi, M. G., Onitsuka, O. & Rubner, M. F. Electroluminescence from CdSe quantum-dot/polymer composites. *Appl. Phys. Lett.* **66**, 1316–1318 (1995).
7. O'Regan, B. & Grätzel, M. A low-cost, high-efficiency solar cell based on dye-sensitized colloidal TiO_2 films. *Nature* **353**, 737–740 (1991).
8. Mikulec, F. V. *et al.* Organometallic synthesis and spectroscopic characterization of manganese-doped CdSe nanocrystals. *J. Am. Chem. Soc.* **122**, 2532–2540 (2000).
9. Chiang, C. K. *et al.* Synthesis of highly conducting films of derivatives of polyacetylene, CH_x. *J. Am. Chem. Soc.* **100**, 1013–1015 (1978).
10. Kamat, P. V. Interfacial charge transfer processes in colloidal semiconductor systems. *Prog. Reaction Kinetics* **19**, 277–316 (1994).
11. Miller, R. J. D., McLendon, G. L., Nozik, A. J., Schmickler, W. & Willig, F. *Surface Electron Transfer Processes* (VCH Publishers, New York, 1995).
12. Haddon, R. C. *et al.* Conducting films of C_{60} and C_{70} by alkali-metal doping. *Nature* **350**, 320–322 (1991).
13. Lee, R. S., Kim, H. J., Fischer, J. E., Thess, A. & Smalley, R. E. Conductivity enhancement in single-walled carbon nanotube bundles doped with K and Br. *Nature* **388**, 255–257 (1997).
14. Guyot-Sionnest, P. & Hines, M. A. Intraband transitions in semiconductor nanocrystals. *Appl. Phys. Lett.* **72**, 686–688 (1998).
15. Shim, M., Shilov, S. V., Braiman, M. S. & Guyot-Sionnest, P. Long-lived delocalized electron states in quantum dots: a step-scan Fourier transform infrared study. *J. Phys. Chem.* **104**, 1494–1496 (2000).
16. Norris, D. J. & Bawendi, M. G. Measurement and assignment of the size-dependent optical spectrum in CdSe quantum dots. *Phys. Rev. B* **53**, 16338–16346 (1996).
17. Shim, M. & Guyot-Sionnest, P. Permanent dipole moment and charges in colloidal semiconductor quantum dots. *J. Chem. Phys.* **111**, 6955–6964 (1999).
18. Hoyer, P., Eichberger, R. & Weller, H. Spectroelectrochemical investigations of nanocrystalline ZnO films. *Ber. Bunsenges. Phys. Chem.* **97**, 630–635 (1993).
19. Hoyer, P. & Weller, H. Size-dependent redox potentials of quantized zinc oxide measured with an optically transparent thin layer electrode. *Chem. Phys. Lett.* **221**, 379–384 (1994).
20. Bruchez, M. Jr, Moronne, M., Gin, P., Weiss, S. & Alivisatos, A. P. Semiconductor nanocrystals as fluorescent biological labels. *Science* **281**, 2013–2016 (1998).
21. Chan, W. C. W. & Nie, S. Quantum dot bioconjugates for ultrasensitive nonisotopic detection. *Science* **281**, 2016–2018 (1998).

Acknowledgements

This work was funded by the US NSF. We made use of the Materials Research Science and Engineering Center (MRSEC) shared facilities supported by the US NSF.

Correspondence and requests for materials should be addressed to M.S. (e-mail: mshim@uchicago.edu) or P.G.S. (e-mail: pgs@uchicago.edu).

Three-dimensional control of light in a two-dimensional photonic crystal slab

Edmond Chow*, S.Y. Lin*, S.G. Johnson†, P.R. Villeneuve†, J.D. Joannopoulos†, J.R. Wendt*, G.A. Vawter*, W. Zubrzycki*, H. Hou* & A. Alleman*

* *Sandia National Laboratories, PO Box 5800, Albuquerque, New Mexico 87185, USA*

† *Department of Physics, Massachusetts Institute of Technology, Cambridge, Massachusetts 02139, USA*

Optoelectronic devices are increasingly important in communication and information technology. To achieve the necessary manipulation of light (which carries information in optoelectronic devices), considerable efforts are directed at the development of photonic crystals—periodic dielectric materials that have so-called photonic bandgaps, which prohibit the propagation of photons having energies within the bandgap region. Straightforward application of the bandgap concept is generally thought to

Electron Relaxation in Colloidal InP Quantum Dots with Photogenerated Excitons or Chemically Injected Electrons

Jeff L. Blackburn,*,† Randy J. Ellingson,*,‡ Olga I. Micić,‡ and Arthur J. Nozik*,†,‡

Department of Chemistry and Biochemistry, University of Colorado, Boulder, Colorado 80309, and Center for Basic Science, National Renewable Energy Laboratory, Golden, Colorado, 80401.

Received: August 12, 2002; In Final Form: October 30, 2002

Femtosecond transient absorption spectroscopy has been used to characterize charge carrier relaxation from the second excited state (1P) to the first excited state (1S) in colloidal indium phosphide (InP) quantum dots (QDs). A three pulse experiment consisting of a visible pump, infrared pump, and white light probe was used to characterize the relaxation of photogenerated excitons, and the roles of surface chemistry and size were investigated. A two pulse experiment consisting of only the infrared pump and white light probe was used to characterize the relaxation of chemically injected electrons in the absence of holes. In the case of photogenerated excitons, two subsets of QDs were probed in the experiment, corresponding to exciton-confined and charge-separated QDs. The relaxation rates for exciton-confined and charge-separated QDs increase with decreasing QD diameter. The relaxation rates obtained for both photogenerated excitons that become charge-separated and chemically injected electrons were slowed by approximately 1 order of magnitude as compared to excitons confined to the QD core.

Introduction

Semiconductor nanocrystals, or quantum dots (QDs), represent a remarkable class of materials with properties that bridge the gap between atomic and bulk systems. Quantum size effects arise when electronic particles are confined by potential barriers to regions of space comparable to or smaller than twice the excitonic Bohr radius. In QDs, three-dimensional confinement transforms the broad density of states characteristic of the bulk into discrete atomlike transitions and leads to a size-dependent blue shift of the semiconductor band gap. The potential and realized applications of QDs include photovoltaic cells,[1−4] fluorescent biological labels,[5,6] light-emitting diodes,[7] and QD lasers.[8]

The dynamics of charge carriers within QDs is important from both the standpoint of device performance and the general photophysics of these zero-dimensional systems.[9] In bulk semiconductors, the valence and conduction bands (CB) consist of a broad, densely spaced population of electronic states. Relaxation of photogenerated electrons proceeds by the emission of phonons, primarily longitudinal optical (LO) phonons, due to the large number of states available for momentum and energy conservation. In nanocrystals, excited states become discrete, adjacent electron levels can be separated by several hundred millielectovolts, and photogenerated electrons and holes form excitons even at room temperature. In the case of InP QDs, the energy separation between the first ($1S_e$) and the second ($1P_e$) electron levels ranges from ~276 (50 Å QD) to ~410 meV (26 Å QD). The energy of an LO phonon in InP is 43 meV, meaning that the $1S_e-1P_e$ energy separation ranges from ~7 to 10 LO phonon energies. Relaxation by phonon emission in these systems, therefore, must occur via the emission of multiple phonons, an inefficient process suggesting a possible "phonon bottleneck", which may slow relaxation. Evidence has been given to support[10,11] and contradict[12,13] the phonon bottleneck; additionally, previous research has suggested a dependence on the type of phonon emitted[14] or the carrier involved.[15]

The QD surface has been shown to have a significant effect on the electronic properties of the nanocrystal. Some processes by which electrons in excited states in QDs may bypass the phonon bottleneck are defect-related processes[16] and Auger-like processes[12,17] both of which should be strongly dependent on the QD surface. Auger-like relaxation is based on the electron−hole Coulomb interaction and involves a rapid transfer of excess electronic energy to the hole, which may quickly relax through the dense spectrum of VB states.[17] Coulomb interactions scale inversely with the electron−hole separation, meaning that the efficiency of Auger-like relaxation should be reduced if either carrier is ejected from the QD or becomes localized on the surface of the QD.[12] Detailed studies of excitonic relaxation are necessary to determine the effect of surface chemistry, QD size, and carrier−carrier interactions on excitonic relaxation. Of particular interest are studies on colloidal QDs where either the electron or the hole is quenched by an acceptor molecule.[10,12,18,19] These studies are very useful in assigning spectral and dynamical signatures of electrons, holes, or correlated electron−hole pairs.

Steady state[20−22] and time-resolved[10,12,23−26] experiments have been performed on a variety of semiconductor QDs to explore intraband transitions involving quantized electronic states. These experiments have revealed a great deal about the nature of these transitions and their implications on mechanisms for carrier relaxation. While much attention has been given to II−VI QDs, less work has been done on III−V nanocrystals. We report on time-resolved intraband experiments on strongly confined InP QDs ranging from 26 to 50 Å in diameter. To determine the role of the surface in carrier relaxation dynamics, as-prepared nanocrystals capped in trioctylphosphine (TOP)/trioctylphosphineoxide (TOPO) are compared to TOP/TOPO-capped QDs etched with HF and to pyridine-capped QDs. To examine the

† University of Colorado.
‡ National Renewable Energy Laboratory.

10.1021/jp026746w CCC: $25.00
Published on Web 12/10/2002

role of electron−hole interactions in the relaxation process, it is advantageous to track the relaxation of individual carriers. To this end, the dynamics of chemically injected electrons were examined to elucidate the role of the hole in electronic relaxation. By using infrared transient absorption (TA) spectroscopy, we are able to resolve with clarity two systems: QDs with excitons confined to the interior of the nanocrystal and QDs with holes either absent or localized at surface states. The presence of the hole in the core of the nanocrystal facilitates relaxation, and relaxation in the absence of the hole is slowed by approximately an order of magnitude.

Experimental Section

Synthesis and Surface Preparation of InP Nanocrystals. Indium phosphide QDs were synthesized by standard colloidal methods as previously reported.[27] The reaction mixture, which consists of indium oxalate, trimethylsilylphosphine, and a 0.1:1 ratio of TOP and TOPO, was heated at 250−290 °C for 3 days, yielding an optically transparent colloidal solution. Size selective precipitation with anhydrous methanol was used to achieve a size distribution of roughly ±10%, with this size distribution generally being narrower for samples with larger mean diameters. The TOP/TOPO capping group confers solubility to the QDs in organic solvents and partially passivates QD surface states. Band edge luminescence of TOP/TOPO-capped QDs remains low, however, unless the dots are etched in a dilute butanolic or ethanolic solution of HF.[27] Etching increases the near band edge photoluminescence by a factor of 10 or more and reduces the near-infrared emission associated with deep surface state recombination. The TOP/TOPO capping group is exchanged for pyridine by heating a dried aliquot of the QDs in ~3 mL of pyridine at 60−70 °C for over 2 h and then letting this solution react at room temperature for ~24 h. Addition of hexane precipitates the pyridine-capped dots, which may be centrifuged and resuspended in pyridine.

Preparation of *n*-Type Nanocrystals. These preparations must be performed in a purged drybox as *n*-type nanocrystals are quickly oxidized with exposure to air. As-prepared TOP/TOPO-capped InP QDs were dispersed in approximately 0.3 mL of 2,2,4,4,6,8,8-heptamethylnonane (HMN). The concentration of the solution was adjusted so that the optical density at the first excitonic peak in the linear absorption spectrum was between 0.3 and 0.6 with a path length of 500 μm. Lower optical densities result in weaker signals for the IR-pumped intraband transition, but if the optical density is too high, insufficient transmission of probe light through the sample leads to poor signal-to-noise. To this solution was added approximately 50 μL of 1.2 M sodium biphenyl, and the solution was vigorously stirred with a metal spatula. The solution was then quickly injected into an infrared cell for linear and TA measurements. The infrared cell consisted of two sapphire windows separated by a 0.5−0.95 mm Teflon spacer and capped with Teflon stopcocks.

Steady State Absorption Measurements. Steady state absorption measurements were made using a Cary 500 double beam spectrometer at a spectral resolution of 1 nm.

TA Measurements. TA experiments were performed on QD samples dispersed in hexane, toluene, or HMN, depending on the specific experiment. No differences, spectral or dynamical, were observed among the three solvents. The TA setup was described previously.[28] Briefly, a regeneratively amplified Ti:sapphire laser, operating at 989 Hz and 775 nm, is used to pump visible and infrared optical parametric amplifiers (OPAs), which are used as the experimental pump beams. The IR OPA provides tunable near-IR pulses from 1.1 to 2.5 μm; the signal and idler pulses from the IR OPA are combined in a $AgGaS_2$ crystal to generate mid-IR pulses from 3 to 10 μm by difference frequency generation. Focusing a few milliwatts of the 775 nm beam onto a 2 mm sapphire window generates the white light (WL) continuum probe.

Intraband transitions in neutral QDs coupling the first and second CB levels are accessed via a three pulse configuration, as described in ref 12. In this configuration, the visible pump pulse creates an electron−hole pair in the lowest excited state (1S) of the QD. The energy of the visible pump is chosen such that the photogenerated exciton was no more than 150 meV excess kinetic energy above the first excitonic energy for all samples: $E_{h\nu} - E_{1S} \leq 0.15$ eV. The infrared photon energy is set to be resonant to the S−P energy spacing, which is determined experimentally as the energy difference between the peaks of the 1S and 1P exciton bleaches in the TA spectra. By establishing the S−P energy spacing in this manner, the infrared pulse excites the exciton from the 1S state to the 1P state, since the absorption spectra of QDs reflect transitions between energy states of confined electron−hole pairs.

The primary species measured by the TA bleaching is important to understand for the analysis of the intraband relaxation. Taking into consideration the hole's larger effective mass and closely spaced energy levels near the valence band edge, as well as the relative energy spacings of the CB and valence band (VB) levels, electrons are expected to dominate the dynamics of the TA signal. Thus, while the exciton is the primary excitation in the experiment, electrons dominate the dynamics that were measured. In QDs where the hole becomes trapped or an electron is chemically injected (discussed next), the electron is excited from its lowest level ($1S_e$) to its next higher level ($1P_e$). In these cases, the infrared excitation is slightly off resonance with the $1S_e-1P_e$ energy spacing. However, because of the energetic dispersion of the IR pump and energy level broadening, sufficient absorption of the IR excitation occurs within the sampling volume measured. To simplify the discussion of the three pulse experiment and because electrons should dominate the band edge bleaching, the primary excitation induced by the infrared pulse will be attributed to the electron in all cases. Thus, we will denote electron levels as S_e, P_e, and D_e and excitonic states as S, P, and D.

After some delay with respect to the visible pump pulse, Δt_{IR}, the IR pump pulse promotes the $1S_e$ electron to the $1P_e$ level. The WL probe monitors the bleaching of the 1S transition, so that if the IR pump beam is chopped, the differential absorption resulting from only those electrons excited by the IR pump is monitored. To obtain dynamical data for electrons involved in the intraband transition, the visible and IR pump pulse are set to the desired relative delay, Δt_{IR}. The interband probe pulse is then delayed relative to the fixed pump pulses using an optical delay line capable of up to 300 ps delay. The delay of the interband probe pulse with respect to the visible pump will be denoted t_{pr}.

The pump fluence of the visible pump was kept low enough so that the average initial photogenerated exciton population was kept at 0.5 excitons per QD or less to avoid multiexciton interactions.[28] Depending on the IR pump fluence, anywhere from 15 to 50% of the electrons initially created by the visible pump pulse were reexcited by the IR pump pulse. Experiments were performed on one sample at several different IR pump fluencies, adjusted by attenuation of the IR beam, to see if this variance affected experimental results. No dependence on the

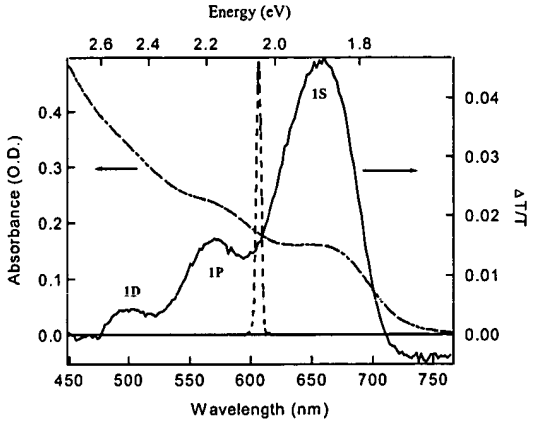

Figure 1. Linear absorption spectrum (dash-dotted line) and TA spectrum (solid line) for excitation at 3.2 eV, t_{pr} = 500 fs. The dashed line shows the excitation pulse used in the three pulse experiment. A good size distribution for this 43 Å sample allows for the identification of three distinct transitions: 1S (1.89 eV), 1P (2.17 eV), and 1D (2.49 eV). Spectra taken on samples with broader size distributions show broader, more poorly defined features.

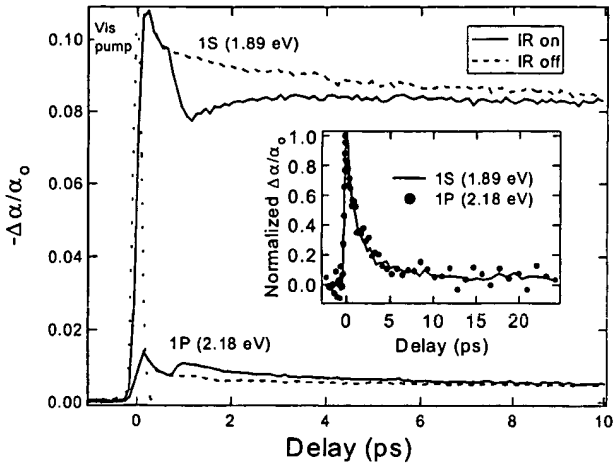

Figure 2. 1S and 1P bleaching dynamics measured with IR pump off (dashed lines) and IR pump on (solid lines) for 43 Å InP QDs. Note small bleaching signal at 1P transition prior to IR pump even though the visible pump does not populate this state. This bleach is due to the Stark effect created by the 1S electron. Inset: Normalized IR-modulated 1S bleach recovery and 1P bleach decay (sign reversed).

dynamics of relaxation with respect to IR pump fluence was observed, so all experiments were performed under conditions of the maximum IR pump fluence attainable to ensure the largest possible signal-to-noise.

The same intraband transition may be accessed in the *n*-type nanocrystals with only the IR pump pulse. In these QDs, an electron has been injected chemically into the CB by the biphenyl anion, which has a large negative redox potential; therefore, photogeneration by the visible pump pulse is unnecessary. Thus, dynamic TA experiments on *n* type nanocrystals are obtained by varying the delay of the WL probe pulse while keeping the position of the IR pump pulse fixed.

Spectral data were obtained for neutral or *n*-type nanocrystals by maintaining a fixed relative delay for the probe pulse and pump pulse(s), while spectrally dispersing the probe pulse using a CVI DK240 0.25 m monochromator.[28] All spectra were corrected for the chirp of the probe beam. The chirp was determined experimentally by measuring two photon absorption with the visible pump and the WL probe in a ZnO crystal. The wavelength-dependent chirp correction was entered into a table, which was used to correct spectra during acquisition.

Results and Discussion

Three Pulse Dynamics. Figure 1 shows the linear absorption spectrum of 43 Å TOP/TOPO-capped InP QDs (dash-dotted line) and the TA spectrum (solid line) taken 500 fs after excitation at 3.2 eV. The dashed line shows the visible excitation pulse used in the three pulse experiment for this sample. The first excitonic transition appears as a broadened peak in the linear absorption spectrum around 1.9 eV, followed by broad shoulders corresponding to two higher energy transitions. Electronic occupation of discrete states, or state filling, leads to absorption bleaches at the positions of these transitions in the TA spectrum. Three well-resolved transitions are seen in the TA spectrum at 1.89 (1S), 2.18 (1P), and 2.49 eV (1D). The parenthetical name given to each transition is based on recent theoretical calculations, which determined the dominant character (s, p, and d, respectively) for each transition in a 42 Å InP QD.[29] In QD samples with mean diameters smaller than ~36 Å, only the first excitonic transition is discernible in the TA spectrum. The energy spacing between the first two transitions is calculated from the value of the corresponding bleaches and for this sample is 0.29 eV. The induced absorption occurring to the red of the 1S bleach at ~1.75 eV is attributed to the carrier-induced Stark effect, resulting from the initially created exciton shifting the 1S transition to lower energy.[30] At later times, a relatively flat absorption persists below 1.75 eV and stretches into the infrared; this feature is attributed to excited state absorption.

The visible pump pulse in the three pulse experiment is used to create electrons in the lowest unoccupied electron level ($1S_e$) to be subsequently pumped by the IR pump pulse to the next highest electron level ($1P_e$). The energy of the visible photon is such that electrons are created only in the $1S_e$ level for the majority of QDs within the sample and not in the $1P_e$ level, and the energy of the IR photon is adjusted to match the energy spacing between these levels calculated from the TA bleaching. For the sample shown in Figure 1, excitation at 2.04 eV ensures that electrons are created only in the $1S_e$ level for the majority of the QDs, and IR excitation at 0.29 eV promotes the electron to the $1P_e$ level. Probing at the energy of the 1S exciton absorption (1.89 eV for this sample) ensures that we only monitor relaxation dynamics of QDs with their 1S excitonic transition at this energy, corresponding to 43 Å diameter QDs.

The dynamics of electrons reexcited by the IR pulse may be obtained in one of two ways, as shown in Figure 2. In one method, the visible pump pulses are chopped and separate scans are taken with the IR pump on and off. Subtraction of these two scans yields the dynamics of only the electrons reexcited by the IR pulse. In the other method, the IR pulse is chopped, giving the direct dynamics of only those electrons reexcited by the IR pulse. Both methods yield the same dynamics, but IR modulation yields better signal-to-noise and is used for the entirety of these experiments.

Excitation of the $1S_e$ electron with the infrared pump leads to a reduction in the bleaching of the 1S exciton absorption corresponding to a transition from the $1S_e$ level and an increase in the bleaching of the 1P absorption corresponding to a transition to the $1P_e$ level (Figure 2). The recovery (decay) of the 1S (1P) bleach corresponds to the intraband relaxation of the IR excited electrons. The inset of Figure 2 shows the normalized IR-modulated dynamics of the increase in 1P bleaching (symbols, sign reversed) and the decrease in 1S bleaching (solid line) for this 43 Å TOP/TOPO-capped InP QD sample. The dynamics of the 1S bleach recovery match the

dynamics of the 1P bleach decay and may be fit to a double exponential. The equivalent dynamics of the two processes underscores one advantage of the three pulse method for observing intraband dynamics. In normal pump−probe TA experiments, processes parallel to state filling obscure the comparison of the 1P bleach decay to the rise time of the 1S bleach. For example, the carrier-induced Stark effect contributes a fast initial rise time to the bleaching of the 1S transition, so to get realistic time constants, the relative contributions of state filling and the Stark effect must be accurately known and accounted for. This is a difficult task, and to date, the rise time of the 1S bleach has not been shown to match the decay of the 1P bleach for our InP QDs. Also, any long time constants involved in $1P_e-1S_e$ relaxation are difficult to extract from the rise time of the 1S bleach due to convolution with the decay of the 1S bleach from recombination. As demonstrated by Figure 2, the three pulse experiment alleviates these problems, yielding dynamics that accurately reflect the intraband relaxation of electrons.

Relaxation is well fit with a double exponential, indicating the existence of two possible relaxation pathways or the existence of two subsets of excitations probed in the experiment. The coefficients for the double exponential decay for the 43 Å sample shown in Figure 2 are 540 fs (67%) and 4.0 ps (33%). With the 0.29 eV S−P energy spacing for these nanocrystals, these time constants correspond to relaxation rates of 0.54 and 0.073 eV ps^{-1}, which are close to relaxation rates obtained for strongly confined CdSe QDs.[10,12] Those authors, however, also observed a very long time constant for S−P relaxation corresponding to $\sim 10^{-3}$ eV ps^{-1}, which we do not observe. This slow relaxation was attributed to either a phonon bottleneck in charge-separated QDs[10] or the accumulation of electrons in high-energy long-lived states accessed by nonlinear IR excitation.[12]

In ref 12, Klimov used a three pulse experiment similar to the one described here and found strongly reduced electron cooling rates when holes were captured by pyridine capping molecules after 430 fs. In this case, the relaxation time constant increased from 0.25 to 3 ps, indicating a transition from an exciton-confined QD to a charge-separated QD with the hole localized on the pyridine capping molecule. It is interesting to note the similarity of the relaxation rates obtained in refs 10 and 12 to the rates obtained on our InP QDs. This suggests the possibility that the time constants obtained in our experiments reflect two subsets of excitations probed in the experiment, corresponding to exciton-confined and charge-separated QDs. This possibility will be discussed further in the next section.

Surface Chemistry and Charge Separation. To investigate the role of charge separation in intraband relaxation, three different surface chemistries were explored as follows: TOP/TOPO-capped InP, HF-etched TOP/TOPO-capped InP, and pyridine-capped InP. Passivation with pyridine quenches band edge PL, ostensibly because of hole transfer to the pyridine molecule, which can readily stabilize the positive charge on the aromatic ring. In a three pulse experiment similar to ours, Klimov found that hole transfer to pyridine capping molecules on CdSe QDs occurred in 430 fs, as evidenced by the time dependence of the electron relaxation rate on the delay of the IR pump.[12] In Klimov's experiment, as the IR pulse was delayed from 75 to 430 fs with respect to the visible pump beam, the electronic relaxation time constant gradually increased from 250 fs to 3 ps; at a delay of 430 fs or longer, the time constant remained at 3 ps. The same experiment was performed on our InP QDs by varying Δt_{IR} from 75 fs to 3 ps on QDs with all three surface chemistries described above. One would expect

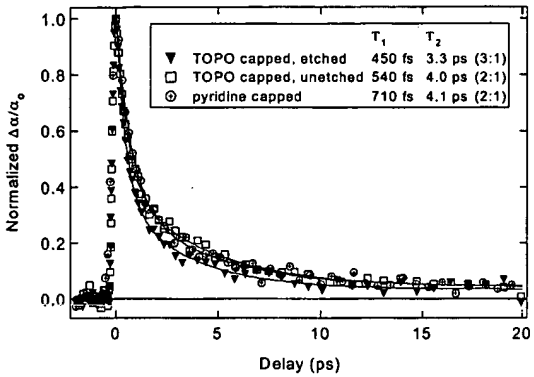

Figure 3. Normalized recovery of 1S bleaching in three pulse experiment for 43 Å InP QD sample with three different surface chemistries. Symbols are data, and solid lines are biexponential fits. Time constants are shown in the inset with the amplitudes for each time constant given in parentheses.

to see a relaxation rate dependent on Δt_{IR} for the pyridine-capped QDs if charge separation should occur and not in the case of etched or unetched TOP/TOPO-capped QDs where no charge separation is expected.

Surprisingly, it was found that the relaxation rate was completely independent of Δt_{IR} for all three surface chemistries examined in this study. At all IR pump delays, relaxation was biexponential with a ~500−750 fs time constant and ~2−4 ps time constant. With regards to a hole-trapping time scale, this implies that the hole either is never trapped or is trapped within the first 75 fs (the shortest Δt_{IR} studied) after photoexcitation. This lack of time dependence was expected for etched and unetched TOP/TOPO-capped QDs but is rather surprising for pyridine-capped QDs. What is also surprising is that the surface chemistry of the QD seems to play little role in the relaxation rate. Figure 3 shows the recovery of the 1S bleach for 43 Å InP QDs with the three different surface chemistries. All scans shown are taken at an IR pump delay of 1 ps, but it is important to remember that a scan taken at any Δt_{IR} shows the same dynamics due to the lack of time dependence. Here are three samples with very different PL quantum yields, indicative of differences in carrier trapping, but all samples show the same biexponential behavior for intraband relaxation, with slight differences in time constants for these particular scans.

The dynamics for the etched sample show a slightly higher magnitude, 75%, for the faster time component. Because the etching process increases emission by passivating surface carrier traps more completely than organic passivation, this increase suggests that the fast component of relaxation may be representative of "higher quality" QDs with more completely passivated surfaces. The results of these three pulse experiments may be compared to recent electron paramagnetic resonance (EPR) and optically detected magnetic resonance (ODMR) results[31,32] to gain some insight into the nature of this passivation and the effect on intraband relaxation. It was originally believed that etching with HF greatly increased band edge emission by passivating electron and hole traps at the surface with F^- and H^+, respectively. Following this logic, after successfully etching a sample of InP QDs with dilute HF, it would be expected that both carriers should be efficiently confined to the interior of the nanocrystal. Because of the strong electron−hole wave function overlap, relaxation should be efficient in this scenario. The EPR and ODMR studies elucidated the chemical nature of the QD surface states and their response to HF etching. It was found that two electron traps, related to indium dangling bonds, exist on the surface slightly below the CB in energy, one

radiative and one nonradiative. Etching the QD sample with HF was found to eliminate both of these traps, because of the ability of the small fluoride anion to effectively passivate these dangling bonds. A hole trap consistent with a phosphorus dangling bond was also discovered slightly above the VB. This trap state was not eliminated with HF etching, indicating poor passivation of the phosphorus dangling bonds with H^+.

The results of these experiments suggest that the severalfold increase in PL from HF etching is a result of efficient passivation of electronic surface states, but a permanent hole trap still exists on the surface of the InP QDs. Also very important is the fact that not all QDs within a given sample will possess each kind of trap. Variation of QD quality within a sample has been seen for CdSe QDs in electrostatic force microscopy (EFM) experiments performed by Krauss et al.[33] Those authors found that photoionization events in ~50% of the CdSe QDs within their samples left a positive charge on these nanocrystals' surfaces, indicative of a surface-localized hole.

Applying these results to the dynamics shown in Figure 3, a possible model for intraband relaxation is proposed. If HF etching passivates electronic surface states but not hole surface states, then the hole can become localized at the surface in both etched and unetched TOPO-capped QDs, and the dynamics associated with these two samples will not deviate significantly. The fact that the relaxation is biexponential suggests the possibility of two subsets of QDs within the sample. Because etching has been shown to inefficiently passivate hole traps, it is proposed that two subsets of QDs are probed in this experiment: one subset in which the hole and electron are efficiently confined to the interior of the nanocrystal (hole trap absent; exciton-confined QD) and one subset in which the hole is localized at the surface of the QD on a phosphorus dangling bond (hole trap present; charge-separated QD).

With the electron and hole confined to the QD core, strong electron–hole interaction leads to efficient, fast relaxation, and in QDs where the hole is localized at the surface, increased spatial separation results in slower relaxation. The relaxation is consistent with Coulomb interaction-mediated electron–hole energy transfer proposed in previous work on CdSe[12,17] that occurs with reduced efficiency when the hole is trapped at the surface of the QD. The slightly larger magnitude for the fast time component for the etched sample implies that the etching process may partially passivate the hole traps. The fact that no time dependence is observed in the dynamics down to 75 fs implies that trapping at this intrinsic surface state occurs in less than 75 fs. The lack of a significant effect on coordinating ligand (i.e., TOPO and pyridine) suggests that unlike the case of CdSe QDs, holes are not trapped by pyridine in the time scale studied (75 fs to 3 ps). Electrochemical experiments on pyridine suggest that oxidation occurs around +1.6 V vs NHE.[34] The differing ability of pyridine to trap holes may result from the relative energetics of the VB minimum (VBM) for CdSe and InP QDs. Also possible is that hole trapping by pyridine, in contrast to trapping at P dangling bonds, occurs on a slower time scale in InP QDs than examined in this study (i.e., >3 ps). Further research is necessary to elucidate the actual quenching mechanism.

The response of the intraband dynamics to oxidation of the sample also supports the hypothesis that the slow component of relaxation results from hole trapping at P dangling bonds. EPR results show that adsorption of oxygen to the QD surface affects the hole trapping sites,[32] and it has been shown by X-ray photoelectron spectroscopy that oxygen directly binds to surface phosphorus atoms, passivating hole traps associated with P dangling bonds.[35] With regards to the intraband dynamics examined in this paper, the passivation of the surface hole traps by oxidation should lead to a decrease in the magnitude of the slow time constant in the biexponential P–S dynamics. Figure 4 clearly shows a significant decrease of the magnitude of the ~4 ps time constant upon aging in the presence of air, supporting the assignment of the slow component to QDs where the hole has become trapped at surface P dangling bonds.

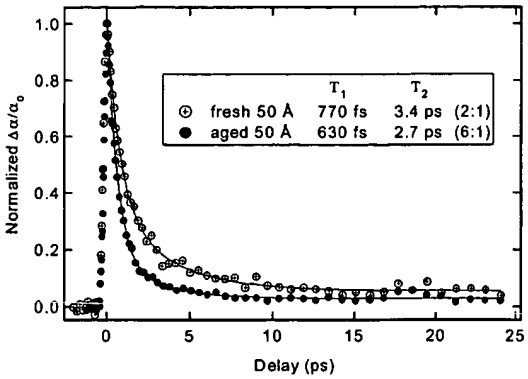

Figure 4. Normalized recovery of 1S bleaching in three pulse experiment for 50 Å TOP/TOPO-capped InP QDs in hexane. The fresh sample was maintained in an oxygen free glovebox and measured immediately in the sealed IR cell. The aged sample was left open to air. Time constants are shown in the inset with the amplitudes for each time constant given in parentheses.

Three Pulse Spectra. It is possible that nonlinear IR absorption, i.e., two photon absorption, can populate higher excited states or interface states that relax to the 1S state more slowly, contributing to the biexponential behavior of excitonic relaxation. The spectral positions of excited states in larger InP QDs allow our TA setup to check for these nonlinear processes. Shown in Figure 5a are TA spectra taken at different relative probe delays ($t_{pr} - \Delta t_{IR}$) on a 50 Å InP QD sample at an IR pump delay (Δt_{IR}) of 3 ps. The inset shows the normal pump–probe TA spectrum as a reference for the bleaching positions induced by the visible pump. Immediately following reexcitation of the $1S_e$ electron by the IR pump, several changes in the transient bleaching spectrum are observed. An increase in absorption is observed as a broad shoulder around 750 nm (1.65 eV), the spectral position of the photoinduced absorption. Adjacent to this, at around 674 nm, is a large induced absorption corresponding to the reduction of the 1S bleaching. This is caused by the IR-induced resonant transition from the $1S_e$ to the $1P_e$ level and interestingly is blue-shifted by ~43 meV from the normal 1S bleach position. After 1.05 ps, the 1S feature has shifted back to its normal position. The reason for the blue shift is unknown, but it interestingly matches the LO phonon energy in InP.

Successful promotion of the electron to the $1P_e$ level creates an IR-induced bleach at 600 nm (2.07 eV) but also induces a bleach at 540 nm (2.30 eV), the position of the 1D. As relaxation progresses, higher energy electrons primarily populate the $1P_e$ level and continually repopulate the $1S_e$ level. Theoretical calculations on a 42 Å InP QD indicate that the 1D peak is made up of three separate excitonic transitions, one of which shares the $1P_e$ electron level with the 1P exciton transition.[29] This implies that if the electron is promoted to the $1P_e$ level, state filling should also produce a partial bleach in the TA spectrum for the 1D peak. This situation is a possibility for the 50 Å InP QD shown in Figure 5.

While this explanation may provide some insight into the origin of the 1D bleach, two photon absorption must also be

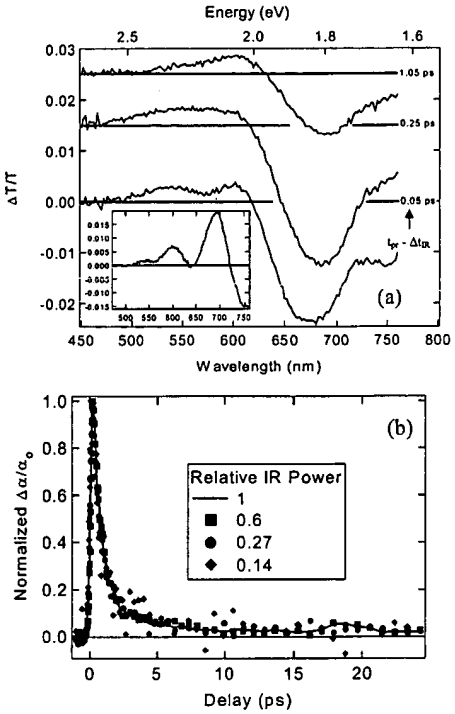

Figure 5. (a) TA spectra showing changes in transmission induced by the IR pump in the three pulse experiment for a 50 Å InP QD sample. Times shown are the probe delay relative to the IR pump. The IR pump is held at a 3.0 ps delay with respect to the visible pump (Δt_{IR} = 3.0 ps), so that $[t_{pr} - \Delta t_{IR}]$ = 0.05 ps corresponds to an absolute WL probe delay of 3.05 ps with respect to the visible pump. Shown in the inset is the normal two pulse TA spectrum taken between 0.1 and 0.5 ps after excitation at 3.2 eV as a reference for the original visible-induced bleaching signals. (b) Intraband dynamics of 50 Å InP QD sample taken at Δt_{IR} = 3.0 ps at different IR pump intensities. Relative IR power is shown in the inset. It should be noted that this sample was slightly oxidized, leading to slightly faster than normal dynamics as discussed in Figure 4.

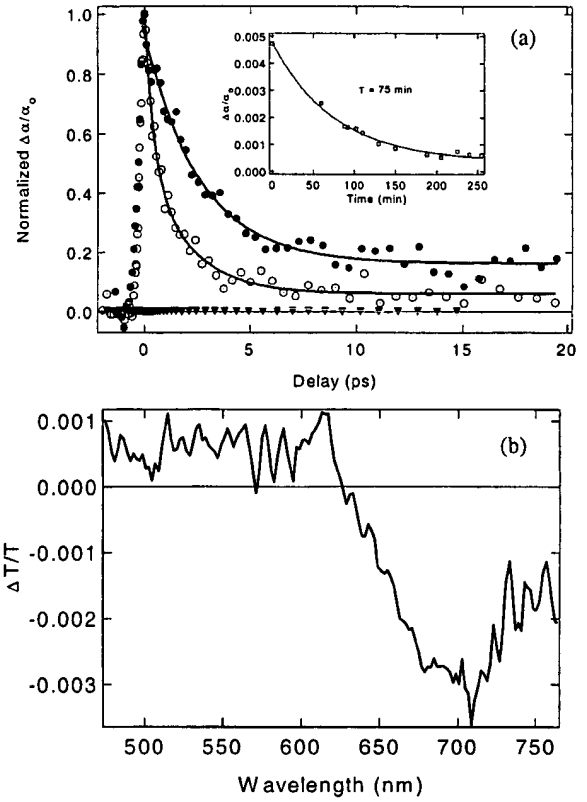

Figure 6. (a) TA traces comparing dynamics of 1S bleach recovery in 50 Å InP QDs. Open circles show neutral QDs where the 1S exciton is created via three pulse experiment. Closed circles show *n*-type QDs where 1S electron is injected chemically and pumped only with IR pulse. Triangles show neutral QDs pumped only with IR pulse. The inset shows the time evolution of the intraband transition signal in *n*-type QDs due to chemically injected electrons. (b) Spectral changes induced by IR pump on 50 Å InP QD treated with sodium biphenyl to inject electrons into the QD CB.

considered. The P−D energy spacing for the larger InP QD samples is quite close to the S−P energy spacing, and for the sample in Figure 5, the two only differ by about 40 meV. It is therefore possible that a two photon absorption process could populate this 1D level, giving rise to the IR-induced absorption at 2.30 eV. The population of higher energy excited states could explain the biexponential behavior of relaxation. Studies on bulk semiconductors have shown that higher energy excitation within the central Γ valley allows access to lower mobility satellite valleys (X and L).[36] In ref 36, carrier mobility in the highly mobile Γ valley of bulk GaAs was measured, and it was found that due to finite scattering rates from satellite valleys back into the Γ valley, higher energy excitation yielded slower signal rise times. This is a feasible scenario for excitations in QDs as well. Recent theoretical calculations have found several L-derived conduction levels at energies between the $1D_e$ and $1P_e$ levels.[29] The contribution of two photon absorption to the dynamics of relaxation may be ruled out, however, by examining the dependence of the dynamics on the power of the IR beam (Figure 5b). It can be seen in this figure that when the IR power is varied over approximately an order of magnitude, the relative contributions of the fast and slow components of relaxation do not change.

***N*-Type Nanocrystals: Relaxation in the Absence of Holes.** To accurately assess the mechanisms involved in the intraband relaxation, it is helpful to view a system in which only one carrier is present. *N*-type nanocrystals represent a system in which electronic relaxation may be measured in the absence of holes. Sodium biphenyl is a very strong reducing agent, which has been shown to successfully inject electrons into the CB of CdSe QDs,[20,21] effectively bleaching the 1S transition and allowing an IR-induced transition to the $1P_e$ level. Steady state absorption and luminescence experiments have elucidated important features about these systems, but to date, time-resolved techniques have not been used to follow the dynamics of the IR-induced intraband transition associated with the injected electron.

Sodium biphenyl was successfully used to inject electrons into the CB of our InP QDs. After a sample of InP QDs is treated with sodium biphenyl, the first excitonic transition is bleached indicating an electron is present in the lowest unoccupied electron level. This $1S_e$ electron may be excited to the $1P_e$ level with the IR pump. Figure 6a compares the dynamics of the time-resolved, IR-induced transitions in *n* type and neutral 50 Å TOP/TOPO-capped InP QDs. In neutral QDs (open circles), where the IR pulse induces the $1S_e-1P_e$ transition on a photogenerated electron, relaxation occurs biexponentially (solid fit line) as expected. Triangles represent the same sample pumped only with the IR pump. No absorption of the IR pump occurs because no electrons are present in the CB. In sharp contrast, only the IR pump is necessary to pump the $1S_e-1P_e$ transition in the same sample treated with sodium biphenyl (filled circles). The relaxation of electrons pumped in this experiment is fit to a single exponential (solid line) with an average time constant of 3.0 ps, corresponding to a relaxation rate of 0.092 eV ps^{-1}.

Figure 6b shows the spectral changes induced by the IR pump 300 fs after excitation. The reduction in bleaching maps out the 1S transition just as in Figure 5a for the 50 Å neutral QDs treated with the three pulse configuration. This confirms that electrons are successfully injected into the QD CB and that the two experiments monitor the same S−P transition.

Shown in the inset of Figure 6a is the disappearance of the IR-induced transition with time. The *n*-type QDs oxidize relatively quickly due to the infiltration of air into the cells, which are not entirely airtight. In the case of our InP QDs, oxidation occurs exponentially with a time constant of 75 min. This presents an experimental challenge in that TA spectra and dynamical scans must be performed immediately following treatment with sodium biphenyl. It has been shown that this oxidation rate is quenched at lower temperatures,[20] although we did not perform any experiments at lower temperatures for this paper.

In *n*-type QDs, no hole is present to facilitate relaxation via Auger-like electron−hole energy transfer. It is therefore expected, and observed, that the fast time constant is absent from the relaxation dynamics. This confirms that in the absence of a core-confined hole, electronic relaxation is slowed by about an order of magnitude. The relaxation rate obtained matches very closely with the relaxation rate assigned to electronic relaxation with a surface-localized hole, suggesting a similar relaxation mechanism.

A consideration of the physical environment of the QD within the sodium biphenyl-treated solution may yield some insight into this similarity. The sodium biphenyl is initially dissolved in di(ethyleneglycol) diethyl ether, which has a high dielectric constant. This solution is vigorously stirred into a solution of HMN, which has a much lower dielectric constant of ~2.0. Because the biphenyl anion is in large excess as compared to the QDs and the redox potential is far negative of the QD CB, electrons should be injected into the QD CB as well as electronic traps associated with the surface states mentioned earlier. This should leave an overall negative charge on the QD surface. Because of the very low dielectric constant of HMN, sodium ions are likely to associate with the negatively charged QD surface. Hence, even though no photogenerated holes are present in the *n*-type QD, electronic relaxation may be affected by the positive charge localized at the QD surface, creating a situation analogous to relaxation in neutral QDs with a surface-localized hole. Thus, similar Coulombic coupling associated with a surface-localized positive charge may be present in both cases, leading to similar relaxation rates.

Another interesting feature of the dynamics for the *n*-type InP QDs is that the 1S bleach does not fully recover following IR excitation on the time scale studied here. This could be indicative of a very slow time constant for the $1P_e-1S_e$ relaxation that we cannot resolve due to the time constraints of the experiment mentioned above. This could result from a variation in the distribution of surface electron traps within the QD sample similar to the hole trap distribution discussed above. In this case, QDs without surface electron traps would not be left with an overall negative surface charge and would not have sodium ions associated with the surface. Thus, electronic relaxation would occur in the complete absence of Coulombic coupling, leading to slow relaxation via a phonon bottleneck. The incomplete 1S bleach recovery could also be indicative of an increased probability of photoionization due to nonlinear IR excitation in the *n*-type QDs. It is feasible that the lack of a hole in the QD could make ejection of the electron into the solvent easier than for the case where the hole is present. Neither of the above hypotheses may be confirmed from these experiments and further experiments, likely at lower temperatures, are necessary to investigate this interesting feature.

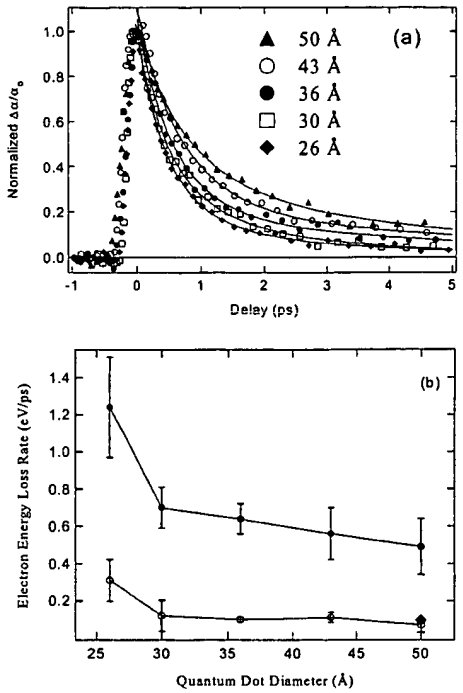

Figure 7. (a) Normalized recovery of 1S bleaching in three pulse experiment for five InP QD samples with different mean diameters. Symbols are data, and solid lines are biexponential fits. (b) Exciton energy loss rate as a function of QD diameter. Calculated using average values for biexponential fit and energy spacing between 1S and 1P transition. The slow component is shown as open circles, and the fast component is shown as closed circles. Also shown as the filled diamond is the energy loss rate for CB electron in *n* type QDs.

Size Dependence of Intraband Relaxation. The model for the phonon bottleneck predicts that in smaller QDs where the $1S_e-1P_e$ spacing becomes much larger, phonon effects may play a greater role in electronic relaxation, leading to slowed relaxation. To examine this possibility, a series of five InP QD samples ranging from 26 to 50 Å in diameter was examined with the three pulse experiment. For each sample, the photon energy of the IR pump was adjusted to be resonant with the S−P transition. For the smallest two sizes, the size distribution was too broad to observe a well-defined peak for the 1P transition. For these samples, the S−P energy spacing measured on samples of narrower size distribution in ref 37 was used. Figure 7a shows the three pulse dynamics for the five different-sized samples taken at an IR pump delay of 1 ps. As previously observed, no samples showed any time dependence of the relaxation on the IR pump delay, and all of the decays fit well to a double exponential (solid lines). Figure 7a unambiguously demonstrates a decrease in the relaxation time constants (i.e., increase in relaxation rates) with decreasing size.

Figure 7b summarizes the dependence of the fast and slow relaxation rates on QD size. Also shown as the diamond is the relaxation rate obtained for electrons in the 50 Å *n*-type QDs discussed in the previous section. Both rates increase with decreasing dot size, although the slower rate increases less rapidly. That both rates increase with decreasing QD size supports the hypothesis that the relaxation in both exciton-confined and charge-separated QDs is mediated by Coulomb electron−hole interactions. The issue of why relaxation in the

in *n*-type QDs does not proceed more slowly than ~3 ps is a very important one that must be further explored.

Conclusion

We have demonstrated the successful injection of electrons into the CB of InP QDs and the temporal tracking of these injected electrons by TA spectroscopy. The comparison of the dynamics of chemically injected electrons to the dynamics of photogenerated electrons shows a reduction in the electron relaxation rate by approximately 1 order of magnitude when the hole is absent or trapped at the surface of the QD. It is proposed that an intrinsic surface state related to phosphorus dangling bonds acts to trap photogenerated holes. Our results suggest that the different surface preparations for the InP QDs primarily affect midgap electron trapping sites, producing only slight variations in electronic relaxation within the CB. The size-dependent dynamics of the 1P−1S relaxation indicate relaxation rates that increase with decreasing dot size.

Acknowledgment. We thank the U.S. Department of Energy, Office of Science, Office of Basic Energy Sciences, Division of Chemical Sciences, Geosciences, and Biosciences for financial support and Garry Rumbles for helpful discussions.

References and Notes

(1) Zaban, A.; Mićić, O. I.; Gregg, B. A.; Nozik, A. J. *Langmuir* **1998**, *14*, 3153.
(2) Greenham, N. C.; Poeng, X.; Alivisatos, A. P. *Phys. Rev. B* **1996**, *54*, 17628.
(3) Greenham, N. C.; Peng, X.; Alivisatos, A. P. *Phys. Rev. B* **1999**, *59*, 10622.
(4) Vogel, R.; Weller, H. *J. Phys. Chem.* **1994**, *98*, 3183.
(5) Bruchez, M., Jr.; Moronne, M.; Gin, P.; Weiss, S.; Alivisatos, A. P. *Science* **1998**, *281*, 2013.
(6) Michalet, X.; Pinaud, F.; Lacoste, T. D.; Dahan, M.; Bruchez, M. P.; Alivisatos, A. P.; Weiss, S. *Single Molecules* **2001**, *2*, 261.
(7) Dabbousi, B. O.; Bawendi, M. G.; Onitsuka, O.; Rubner, M. F. *Appl. Phys. Lett.* **1995**, *66*, 1316.
(8) Eisler, H.-J.; Sundar, V. C.; Bawendi, M. G.; Walsh, M.; Smith, H. I.; Klimov, V. *Appl. Phys. Lett.* **2002**, *80*, 4614.
(9) Nozik, A. J. *Annu. Rev. Phys. Chem.* **2001**, *52*, 193.
(10) Guyot-Sionnest, P.; Shim, M.; Matranga, C.; Hines, M. *Phys. Rev. B.* **1999**, *60*, R2181.
(11) Murdin, B. N.; Hollingworth, A. R.; Kamal-Saadi, M.; Kotitschke, R. T.; Ciesla, C. M.; Pidgeon, C. R.; Findlay, P. C.; Pellemans, H. P. M.; Langerak, C. J. G. M.; Rowe, A. C.; Stradling, R. A.; Gornik, E. *Phys. Rev. B* **1999**, *59*, R7817.
(12) Klimov, V. I.; Mikhailovsky, A. A.; McBranch, D. W.; Leatherdale, C. A.; Bawendi, M. G. *Phys. Rev. B* **2000**, *61*, R13349.
(13) Woggon, U.; Giessen, H.; Gindele, F.; Wind, O.; Fluegel, B.; Peyghambarian, N. *Phys. Rev. B* **1996**, *54*, 17681.
(14) Vollmer, M.; Mayer, E. J.; Ruhle, W. W.; Kurtenbach, A.; Eberl, K. *Phys. Rev. B* **1996**, *54*, R17292.
(15) Xu, S.; Mikhailovsky, A. A.; Hollingsworth, J. A.; Klimov, V. I. *Phys. Rev. B* **2002**, *65*, 045319.
(16) Schroeter, D. F.; Griffiths, D. J.; Sercel, P. C. *Phys. Rev. B* **1996**, *54*, 1486.
(17) Efros, A. L.; Kharchenko, V. A.; Rosen, M. *Solid State Commun.* **1995**, *93*, 281.
(18) Burda, C.; Link, S.; Mohamed, M.; El-Sayed, M. *J. Phys. Chem. B* **2001**, *105*, 12286.
(19) Burda, C.; Green, T. C.; Link, S.; El-Sayed, M. *J. Phys. Chem. B* **1999**, *103*, 1783.
(20) Shim, M.; Wang, C.; Guyot-Sionnest, P. J. *J. Phys. Chem. B* **2001**, *105*, 2369.
(21) Shim, M.; Guyot-Sionnest, P. *Nature* **2000**, *407*, 981.
(22) Wang, C.; Shim, M.; Guyot-Sionnest, P. J. *Science* **2001**, *291*, 2390.
(23) Klimov, V. I.; McBranch, D. W. *Phys. Rev. Lett.* **1998**, *80*, 4028.
(24) Shim, M.; Shilov, S. V.; Braiman, M. S.; Guyot-Sionnest, P. J. *J. Phys. Chem. B* **2000**, *104*, 1494.
(25) Shim, M.; Guyot-Sionnest, P. J. *Phys. Rev. B* **2001**, *64*, 245342.
(26) Guyot-Sionnest, P. J.; Hines, M. A. *Appl. Phys. Lett.* **1998**, *72*, 686.
(27) Nozik, A. J.; Mićić, O. I. Colloidal Quantum Dots of II−V Semiconductors. In *Handbook of Nanostructured Materials and Nanotechnology*; Nalwa, H. S., Ed.; Academic Press: New York, 2000; Vol. 3, p 427.
(28) Ellingson, R. J.; Blackburn, J. L.; Yu, P.; Rumbles, G.; Mićić, O. I.; Nozik, A. J. *J. Phys. Chem. B* **2002**, *106*, 7758.
(29) Ellingson, R. J.; Blackburn, J. L.; Mićić, O. I.; Fu, X.; Nozik, A. J. Unpublished results.
(30) Klimov, V. I. *J. Phys. Chem. B* **2000**, *104*, 6112.
(31) Langof, L.; Ehrenfreund, E.; Lifshitz, E.; Mićić, O. I.; Nozik, A. J. *J. Phys. Chem. B* **2002**, *106*, 1606.
(32) Mićić, O. I.; Nozik, A. J.; Lifshitz, E.; Rajh, T.; Poluektov, O. G.; Thurnauer, M. C. *J. Phys. Chem. B* **2002**, *106*, 4390.
(33) Krauss, T. D.; O'Brien, S.; Brus, L. E. *J. Phys. Chem. B* **2001**, *105*, 1725.
(34) Turner, W. R.; Elving, P. J. *Anal. Chem.* **1965**, *37*, 467.
(35) Guzelian, A. A.; Katari, J. E. B.; Kadavanich, A. V.; Banin, U.; Hamad, K.; Juban, E.; Alivisatos, A. P.; Wolters, R. H.; Arnold, C. C.; Heath, J. R. *J. Phys. Chem.* **1996**, *100*, 7212.
(36) Beard, M. C.; Turner, G. M.; Schmuttenmaer, C. A. *Phys. Rev. B* **2000**, *62*, 15764.
(37) Mićić, O. I.; Cheong, H. M.; Fu, H.; Zunger, A.; Sprague, J. R.; Mascarenhas, A.; Nozik, A. J. *J. Phys. Chem. B* **1997**, *101*, 4904.

J|A|C|S
COMMUNICATIONS

Published on Web 06/06/2003

Electron and Hole Injection in PbSe Quantum Dot Films

Brian L. Wehrenberg and Philippe Guyot-Sionnest*

James Franck Institute, The University of Chicago, 5640 South Ellis Avenue, Chicago, Illinois 60637

Received March 28, 2003; E-mail: pgs@uchicago.edu

The ability to dope quantum dots both n- and p-type promises to facilitate the fabrication of several novel optoelectronic devices, just as it did for bulk semiconductors. However, inclusion of a dopant into the interior of a nanocrystal can be difficult, calling for the more direct approach of charge injection. Electrochemical studies have been performed on several nanocrystal systems, including silicon,[1] PbS,[2] CdS,[3] and CdSe.[4] Electrochemistry may allow the determination of the number of charges injected into the nanocrystals; however, it does not distinguish if the charges are injected into delocalized quantum confined states or are placed into localized trap states. In contrast, injection of electrons into quantum confined states of colloidal semiconductor nanocrystals, can be unambiguously confirmed by monitoring changes in both the visible and the IR absorption spectra.[5-7] To date, we know of no studies that have achieved hole injection into quantum confined states and recorded the corresponding spectroscopic changes needed to confirm this fact.

The search for a quantum dot system in which both holes and electrons can be injected into quantum confined states, essentially doping the dots n- and p-type, has lead us to study PbSe quantum dots. It was reasoned that the small band gap of PbSe (0.278 eV at 298 K) should bring both hole and electronic states into the range of stable electrochemical charge injection. In addition, the small effective mass of the charge carriers in PbSe means that well-separated quantum confined states can be obtained for relatively large quantum dots. The larger size might lessen the role of surface trap states, thus favoring the injection of charge into quantum confined states. Here, for the first time, the injection of electrons and holes into quantum confined states of colloidal quantum dots is reported.

The synthesis of PbSe quantum dots capped with oleic acid has been described previously.[8] All measurements are performed in an airtight Teflon electrochemical cell with a ZnSe optical window for spectroscopic measurements. The working electrode is a platinum disk, 1 cm in diameter, with a polished surface treated with a 30 mM solution of 1,6-hexanedithiol in hexane to anchor the dots to the electrode.[9] The thin films of PbSe nanocrystals are drop-cast on the electrode using a 9:1 hexane:octane solution. Shortly after drying, the film is dipped into a 40 mM solution of 1,7-diaminoheptane in methanol for approximately 1 min, heated at 70 °C for 1 h, and then placed under vacuum for several hours to thoroughly dry the film. This treatment is thought to cross-link the quantum dots,[10] and it is repeated two more times. The electrode is then loaded into the electrochemical cell. An Ag wire is used as a pseudoreference electrode. All voltages reported below are relative to this Ag pseudoreference. The electrolyte is an anhydrous 0.1 M solution of $LiClO_4$ in acetonitrile. Preparation of the films and assembly of the electrochemical cell are performed in a glovebox to minimize exposure to oxygen and water. The cell is transferred under nitrogen to an FT-IR spectrometer (Nicolet Nexus 670). The absorption measurements are taken in reflection geometry with the incident beam at 20° from the surface normal of the ZnSe window, against which the working electrode is pressed. All spectroscopic measurements are made 1 min after application of the desired potential to allow for equilibration. All reported optical changes are reversible.

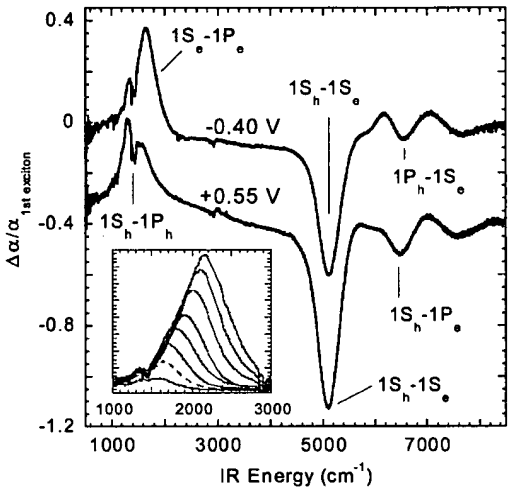

Figure 1. Difference spectra for a film of 7.2 nm diameter PbSe dots at −0.40 and +0.55 V, offset for clarity. The inset shows the induced absorption for a series of voltages between −0.35 and −0.70 V; the dotted line is the feature at −0.40 V. Solvent absorption peaks in the 1000−2000 cm^{-1} range disrupt the induced absorption feature.

Upon injection of a charge carrier into the lowest quantum confined state of a neutral semiconductor nanocrystal, the optical properties of the quantum dot change remarkably. Shown in Figure 1 are the difference spectra between a thin film of PbSe dots under no applied potential and after the application of a positive or a negative potential. The film of 7.2 nm diameter PbSe quantum dots (first exciton at 5100 cm^{-1} at 298 K) has an optical density of 0.015 at the first exciton peak and was determined, by ellipsometry, to have a thickness of approximately 25 nm. Optical studies of the interband and intraband transitions of PbSe have been reported previously[8] and are used here to aid in assignments.

At negative potentials, electrons occupy the $1S_e$ state, and there is a bleach of the interband transitions to that state, accompanied by induced intraband absorptions to higher energy states in the conduction band. At −0.40 V versus the Ag pseudoreference, Figure 1 shows that the first exciton ($1S_h-1S_e$) at 5100 cm^{-1} and the second exciton ($1P_h-1S_e$) at approximately 6600 cm^{-1} are bleached and the intraband ($1S_e-1P_e$) transition at around 1500 cm^{-1} turns on. The robust strength of the 1S−1P interband transitions in PbSe, despite being forbidden by parity, has been observed previously[8] and remains unexplained.

At positive potentials, holes occupy the $1S_h$ state, causing a bleach of the interband transitions involving that state and inducing intraband absorptions to higher energy hole states in the valence

10.1021/ja035369d CCC: $25.00

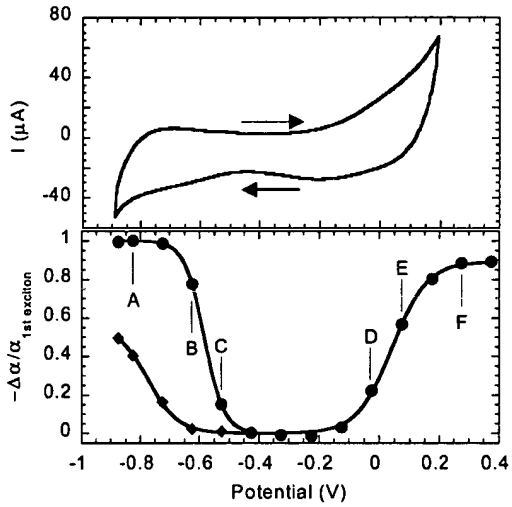

Figure 2. The top panel shows the cyclic voltammetry for a film of 8.8 nm diameter PbSe quantum dots with a scan rate of 17 mV/s. The bottom panel shows the normalized optical bleach of the first (●) and third (◆) excitons, as a function of the applied potential.

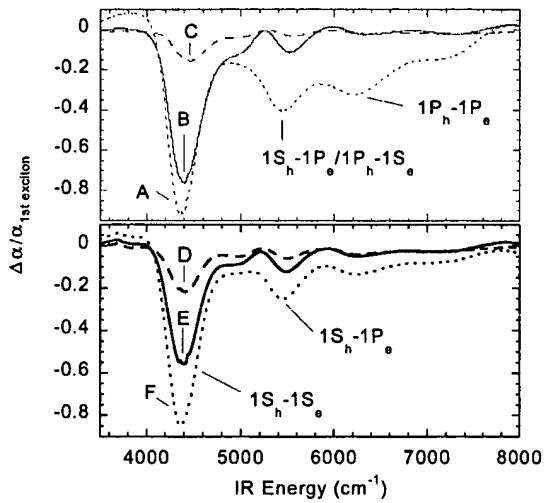

Figure 3. Difference spectra for a film of 8.8 nm diameter PbSe quantum dots taken at the potentials labeled in Figure 2.

band. At +0.55 V, Figure 1 shows the bleach of the first exciton ($1S_h-1S_e$) and the second exciton ($1S_h-1P_e$) around 6500 cm^{-1}. These bleach features are accompanied by an induced absorption feature at around 1400 cm^{-1}, assigned to the $1S_h-1P_h$ intraband transition. Because of the similarity in the effective mass of the electrons and the holes, the electrochromic effects of hole and electron injection appear strikingly similar, with only small shifts in the energies of the transitions.

Figure 2 plots the magnitude of the bleach of the first exciton versus the potential applied to a film of 8.8 nm diameter dots with the first exciton at 4400 cm^{-1} at 298 K. Also shown in Figure 2 is the cyclic voltammetry of the same sample, which demonstrates the correspondence between the reduction and oxidation current waves and the optical bleach. The cyclic voltammetry was stable, showing no variance over several cycles. At potentials more negative than −0.725 V, a 100% bleach of the first exciton is observed. This corresponds to the filling of the $1S_e$ state in all of the quantum dots in the film. The exact number of electrons per dot needed to fill the $1S_e$ state in PbSe nanocrystals is of interest and will be reported in a more detailed investigation. For this sample, the bleach of the first exciton due to hole injection plateaus at ~90%. The application of more positive potentials causes irreversible changes to the film. The voltammetry shows a much more reversible feature for the reduction than for the oxidation, consistent with the lesser stability of the injected hole. Similar behavior is observed for the films of 7.2 nm diameter PbSe nanocrystals; however, for those dots, hole injection bleached the first exciton by ~75%. For dots smaller than those two sizes mentioned here, no significant hole injection was observed, although electron injection was still possible. Injection of charge carriers into higher energy states was only observed for electrons. The magnitude of the bleach of the third exciton ($1P_h-1P_e$) is plotted as a function of the applied potential in Figure 2.

The bleach of the third exciton occurs after the first exciton is completely bleached, demonstrating the sequential filling of first the $1S_e$ and then the $1P_e$ state, separated by ~0.2 V. Figure 3 shows the bleach spectra of the film of 8.8 nm diameter dots, taken at several potentials. The rather dramatic effect that filling the $1P_e$ state has upon the induced absorption can be seen in the inset to Figure 1. The filling of the $1P_e$ state makes the $1P_e-1D_e$ transition available, causing both a blue shift and a large increase of the induced absorption. Neither the change in the bleach spectrum nor the shift of the induced absorption is observed in the hole spectra, indicating that hole injection into states lying higher in energy than the $1S_h$ state does not occur.

We have reported here, for the first time, that both electrons and holes can be injected from an electrode into the quantum confined states of a semiconductor nanocrystal film. While hole injection is less robust than electron injection, this ability should nevertheless allow the development of novel applications, several of which are currently under investigation.

Acknowledgment. We would like to thank the U.S. National Science Foundation (NSF) under grant DMR-0108101 for funding. The authors made use of the MRSEC Shared Facilities supported by NSF under grant DMR-0213745.

References

(1) Ding, Z.; Quinn, B. M.; Haram, S. K.; Pell, L. E.; Korgel, B. A.; Bard, A. J. *Science* **2002**, *296*, 1293.
(2) Chen, S.; Truax, L. A.; Sommers, J. M. *Chem. Mater.* **2000**, *12*, 3864.
(3) Haram, S. K.; Quinn, B. M.; Bard, A. J. *J. Am. Chem. Soc.* **2001**, *123*, 8860.
(4) Myung, N.; Ding, Z.; Bard, A. J. *Nano Lett.* **2002**, *2*, 1315.
(5) Shim, M.; Guyot-Sionnest, P. *Nature* **2000**, *407*, 981.
(6) Wang, C.; Shim, M.; Guyot-Sionnest, P. *Science* **2001**, *291*, 2390.
(7) Wang, C.; Shim, M.; Guyot-Sionnest, P. *Appl. Phys. Lett.* **2002**, *80*, 4.
(8) Wehrenberg, B. L.; Wang, C.; Guyot-Sionnest, P. *J. Phys. Chem. B* **2002**, *106*, 10634.
(9) Colvin, V. L.; Goldstein, A. N.; Alivisatos, A. P. *J. Am. Chem. Soc.* **1992**, *114*, 5221.
(10) Guyot-Sionnest, P.; Wang, C. *J. Phys. Chem. B* **2003**, *107*, ASAP (10.1021/JP0275084).

JA035369D